Master's thesis

NTNU
Norwegian University of Science and Technology
Faculty of Information Technology and Electrical Engineering
Department of Engineering Cybernetics

Torbjørn Yttersian

A tether system for industrial inspection UAVs

Wired power and data

Master's thesis in Industrial Cybernetics
Supervisor: Tor Arne Johansen
July 2019

NTNU
Norwegian University of
Science and Technology

Torbjørn Yttersian

A tether system for industrial inspection UAVs

Wired power and data

Master's thesis in Industrial Cybernetics
Supervisor: Tor Arne Johansen
July 2019

Norwegian University of Science and Technology
Faculty of Information Technology and Electrical Engineering
Department of Engineering Cybernetics

NTNU
Norwegian University of
Science and Technology

Preface

This report is the concluding work of the master's degree program in Industrial Cybernetics at the Norwegian University of Science and Technology (NTNU). The thesis is written in collaboration with Scout Drone Inspection, a spin-off company from the university specializing in autonomous inspection drones.

When Scout offered a chance to work on a tethered power system in relation to an internship, I was immediately interested in the project, especially given my background in power engineering. The process has from start to finish been time consuming and extremely enlightening, with innumerable hours spent figuring out how to design the modules, searching for suitable components, soldering up circuits, plugs and connectors and doing tests runs in the lab. Through this process I have acquired not only a lot of technical knowledge, but also company knowledge by working in a multidisciplinary team, and learned about start-up culture.

The contributions of this thesis lie largely in the analysis around voltage transients, the power quality and stable delivery to the drone, as well as circuit and PCB design. Scout have provided an early conceptual draft of the system and suggested a few key components. They have also reviewed and approved final design choices and assisted in the more advanced assembly processes.

I would like to express my gratitude toward the team at Scout Drone Inspection on the whole for the time I've spent with them, and all the guidance and support they have provided. I would like to thank Nicolai Husteli, for arranging the collaboration and for motivational support. Thanks to Kristian Klausen and Tor Arne Johansen, for technical insight and discussion. Finally, a very special thanks to Kristoffer Slåttsveen and Krzysztof Cisek, for answering both smart and stupid questions, and their invaluable assistance in trivial and important matters.

Trondheim, July 2019

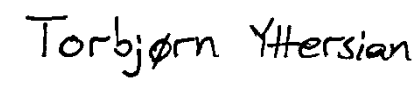

Torbjørn Yttersian

Abstract

This master thesis proposes a complete system that can deliver power to a drone over a high voltage tether. The system includes a safety battery switchover mechanism and is capable of high speed ethernet over the power line. The purpose of the project is to fly an industrial inspection drone without the need to worry about battery life, enabling hours of continuous flight rather than minutes. This thesis discusses the challenges related to such a system and the design considerations that must be made.

The power transmission system is capable of delivering up to 1200 W at 300 V DC to the drone over 30 meters. On the drone this voltage is stepped down to a useable ~19 V by a lightweight but powerful converter chip. One major part of this thesis has been to analyze the power quality and stability of this system. It was discovered that voltage transients would occur when the motors were cut off or changed speed very fast. This transient could potentially damage sensitive equipment on the drone and needed to be addressed. The solution was to use a TVS diode on the ESC to clamp the voltage at a safe level, limiting the transient from up to 23.2 % increased voltage down to 14.1 % in the final system. Additionally, an appropriately sized capacitor on the ESC was found to reduce voltage ripples significantly.

Two backup battery interfaces were designed. One is a passive variant of the diode ORing circuit, with one major advantage being that the backup source can be switched from a MOSFET, reducing losses and increasing flight time on a battery. The other interface is an active variant of the diode ORing circuit with controlled n-MOSFETs, allowing very high efficiency. This variant is part of the final system.

The easy-to-integrate data link is capable of over 90 Mbit/s over the transmission line, even in the presence of noise. This was achieved by adding simple differential mode chokes to the line.

A revised system should upgrade the tether and PSU to 400 V and at least 1.7 kW, since this will enable the 1.5 kW of power available on the drone and reduce transmission losses by up to 47 %.

Contents

Figures

Tables

Acronyms

APU	Air power unit
ESC	Electronic speed controller
HV	High voltage
LV	Low voltage
PSU	Power supply unit
PCB	Printed circuit board
UAV	Unmanned aerial vehicle

Glossary

American wire gauge (AWG)	A logarithmic gauge system for wire diameters, used in North America.
Buck converter	A DC-to-DC converter that steps down voltage and steps up current. The counterpart is the boost converter.
Charge pump	A simple DC-to-DC converter that uses capacitors to boost the voltage.
Reverse polarity protection	A failsafe to protect the electronics in the case of a reverse voltage applied to the terminals, i.e. ground conductor on the V_+ terminal and vice versa.
Through-hole technology (THT)	Electronic components that use leads for mounting to a PCB through holes drilled in the board.

Chapter 1
Introduction

1.1 Background and motivation

Aerial drones have entered the military, consumer and commercial markets exponentially in recent years [1] and defined a new product category and industry in itself. For outdoor applications or indoor open spaces with clear line of sight, battery powered drones have been the convention and are the only realistic solution to long distance operation. In industrial applications, a market has also emerged for short distance, prolonged inspection and surveillance. Such applications include aerial news, media and sports coverage; weather, traffic and crowd monitoring; or lighting and film production to name a few. Due to these tasks often being short distance and operating over hours or even days in the air, a battery pack is unsuitable since flight times vary from 15 minutes to one hour depending on the size of the drone and weight of the payload. The battery may instead be replaced by a physical tether to the ground, which then provides an infinite power source and thus unlimited flight time in theory. Other applications of a tether are missions in environments with limited or blocked wireless signal communication, such as pipelines where a clear line of sight is impossible to maintain. The tether would ensure that a data link to the drone is maintained.

A tethered system is not a new concept, in fact, they are almost exclusively used in underwater drones that require live communication, due to the limited range of wireless signals in water. For aerial drones, tethered commercial solutions are already developed. Elistair [2] and Blue Vigil [3] deliver complete plug-and-play systems featuring tethers up to 100 m in length. The customer can simply replace the battery pack in their existing drones (DJI being the most supported) and enjoy unlimited flight time. UNMND [4] provides a modular, relatively cheap system but requires some know-how from the user and is thus better suited towards hobbyists or developers. Some conceptual systems also use support drones that carry and control the tether, allowing safe operation around for example high voltage power lines without fear of the tether touching the line [5].

Clearly, a market has surfaced for drones in the commercial sector, both battery powered and ground powered. Thus, it is necessary to supply these markets with reliable products.

1.1.1 Scout Drone Inspection

Scout Drone Inspection (“Scout”) is a startup company based in Trondheim and also a spin-off from The Norwegian University of Science and Technology (NTNU). It has started development on an advanced inspection drone, capable of navigating, mapping and inspecting confined spaces where conventional positioning systems are unavailable. Potential applications of such a system include manhole and pipeline inspection, or cargo tank inspection in the maritime industry where currently a lot of dangerous work is carried out by manual workers. These tasks can instead be done by their drone. Currently the drone is designed to run on battery alone, but since its task are largely short distance missions, a tethered solution is of high interest to the company. Figure 1.1 shows a conceptual rendering of a complete product including the tether system.

Figure 1.1: A conceptual rendering of a Scout Drone Inspection quadcopter.
The drone in the back is flying on a tether.

1.2 Description and aim of report

One of the main restrictions upon installing a tether is the weight of the cable and a limited lift capacity in the drone, which restricts the length of the tether and thus the flight radius of the drone. The only real feasible solution to this is to use a high voltage power transmission system in order to reduce the weight of the tether. This requires a converter on board, since the drone itself must operate on low voltage. The other main challenge lies within keeping the power supply stable and reliable, and thus the operation of the drone safe. Voltage transients can be observed when motor throttle is suddenly cut or adjusted in large steps, and this may trigger fuses in the supply line or damage sensitive equipment on board, both of which could be fatal to a drone flying several meters up in the air. It is therefore necessary to use protective circuits and possibly a backup battery system to ensure safe operation of the drone.

This report explores and proposes a complete tethered system for an industrial inspection drone, including onboard converter equipment, a safety battery system and data link over power line. Conditions under which the voltage may spike and the supply become unstable are identified and studied with special emphasis on how to prevent them and improve the power quality. The work carried out is heavily based in practical, tested and observed experiments with components sourced from available shelf products.

1.3 Outline of report and limitations

The report starts with discussing necessary background theory in chapter 2. An introductory draft on a tethered system is presented, along with facts on power transmission and its challenges. Some useful electronic components are also discussed.

Chapter 3 presents the requirements from the company and the hardware that makes the foundation for the system; including the method for component selection and assembly.

Chapter 4 and 5 concerns power quality and stability. A method for quantifying the transient voltages that may occur and how it affects the delivery system is presented. This is followed by an analysis of how protective components can be implemented and how they improve the system. Chapter 4 focuses on a low voltage system used early on to simplify and simulate the drone side of the final system. Chapter 5 focuses on the final system (high voltage), including an analysis of voltage drop and transmission losses over the tether, as well as inrush current challenges.

Chapter 6 presents the flight results with the compounded system on a real drone and discusses how it performs, what worked well and where improvements are necessary.

Finally, the conclusions, recommendations and further work that are of interest to the project are presented in chapter 7.

Due to time constraints, equipment restrictions and lack of technical details regarding components, some boundaries were defined early on when planning the project.

The following was omitted:

- Identifying the exact cause of the voltage transients. Mitigating the problem has instead been prioritized.
- Mathematical analysis of energy released during transients, due to unavailability of data sets.
- Economic comparisons with existing solutions, since this information is classified by the competitors.

Chapter 2
Theory

2.1 High voltage power transmission

In order to understand the motivation behind a high voltage power line, it is necessary to introduce some basic concepts behind electric power transfer.

Electric power can be expressed by the following equations:

$$P = I^2 \cdot R \quad (2.1)$$

$$P = V \cdot I \quad (2.2)$$

where V is voltage, I is current and R is resistance.

Due to internal resistance present in conductors, all wires and power lines will heat up when current passes through them. This lost energy is known as the I^2R *losses* (sometimes called *copper losses*). The power loss is proportional to the square of the current (eq. 2.1), and the current is inversely proportional to the voltage (eq. 2.2) given constant power. Consequently, the transmission losses will be inversely proportional to the square of the voltage, for any constant power output. The downsides to high voltage are increasing demands for insulation and more expensive converter equipment.

For a tethered UAV, the supply is often considered infinite and energy losses are generally not the biggest concern. The length of the tether and thus the reach of the drone will generally be limited by three factors:

- The **heat** generated; although the copper can handle heat well, the insulating material in the tether breaks down at a critical level.
- The **voltage drop** across the tether under load; the equipment on the drone may require a minimum input voltage to operate.
- The **weight** of the tether. The above factors can be compensated for by a larger cross section with less resistance, but the drone has a limited lift capacity.

The common and limiting quantity is the current. A high voltage tether is desirable because it uses fewer amps to do the same work and thus enables lighter wires.

2.2 Concept of tethered system

The basic interface of a tethered system is illustrated in Figure 2.1.

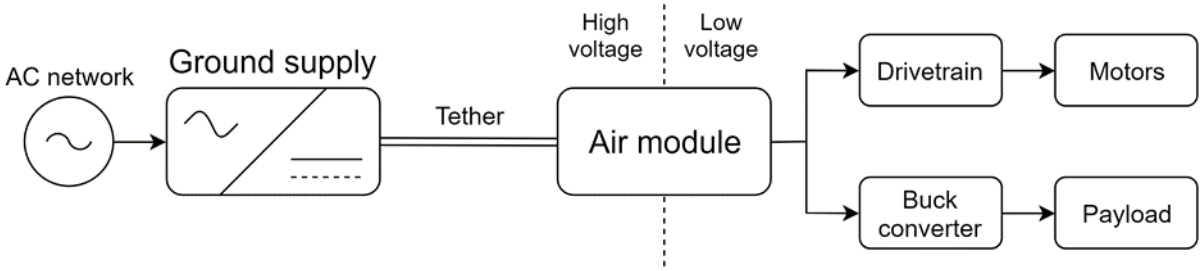

Figure 2.1: Basic concept of tethered system.

It is made up of the following components:

- The ground supply or power supply unit (PSU), connected to the AC grid. It converts AC to high voltage DC[a].
- The tether linking the PSU to the drone. The range will be limited by the factors discussed in the previous section.
- The air module includes the air power unit (APU) which converts high voltage DC to low voltage DC, often equivalent to common battery pack voltages. It may also include a data link interface (ethernet over power line) and a backup battery interface for redundancy.
- The "drivetrain": The electronic speed controller (ESC) and flight controller that drives and controls the BLDC motors. The components listed until now make up the UAVs "powertrain".
- The payload includes all the other equipment onboard: The electronic systems, cameras, sensors etc.

[a] In distribution networks in Norway, high voltage is defined to be higher than 1000 V AC or 1500 V DC. For this paper, high voltage will be considered as anything higher than 100 V.

2.3 Existing tether systems

Several tethered systems have already been developed and are ready for the market. Elistair [2] and Blue Vigil [3] deliver complete systems including a ground box, tether and air module. They already support popular commercial drones on the market from with modules designed to replace the battery pack. These come with winch mechanisms to keep a tension on the tether and also support data transfer over the wire. UNMND develops and delivers a modular kit [4], where the user has more freedom in choosing what parts to include. This solution is better for hobbyists or developers who are making custom drones but don't want to spend the time and resources needed in developing their own technology.

2.4 Surge suppressors

Transient surge suppressors are devices designed to protect sensitive equipment from voltage spikes. They do this by shunting excess current, usually to ground, when the voltage exceeds a certain voltage threshold. This effectively clamps the voltage at a safe level within the device's ratings.

There are many different types of surge suppressors, one of them being the TVS diode ("transient voltage suppressor" or transil diode). The device works similarly to a Zener diode in that it is installed in the blocking direction, which becomes conductive at the breakdown voltage, V_{BR}. The difference is that a Zener diode is intended for constant voltage regulation, while a TVS diode is intended for short bursts of high voltage (in the ns to ms range). See a typical application in Figure 2.2.

The TVS diode has the following key electrical characteristics (see Figure 2.3):

- I_{PP} Peak pulse current, the maximum current at the 10/1000 µs waveform[b].
- P_{PP} Peak pulse power dissipation, the maximum power that can be dissipated.
- V_R Stand-off voltage, maximum voltage that can be applied without operation.
- I_R Leakage current at V_R, usually 1-5 µA.
- V_{BR} Breakdown voltage, at which the diode becomes significantly conductive.
- V_C Clamping voltage, the maximum voltage measured at I_{PP}.

[b] A transient that rises in 10 µs and decays to 50 % value in 1000 µs.

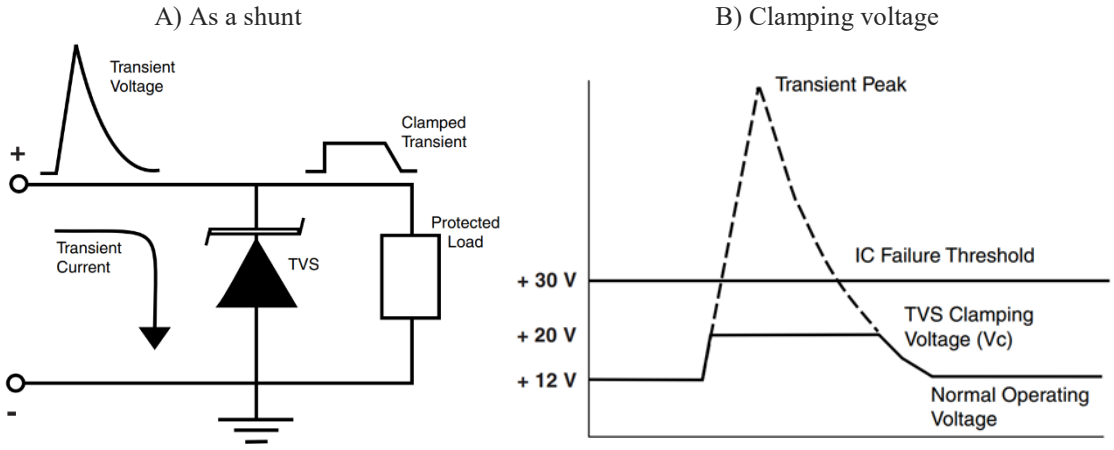

Figure 2.2: Typical application of a TVS diode [6].

When a voltage spike occurs, the excess energy is shunted to ground and the load protected.

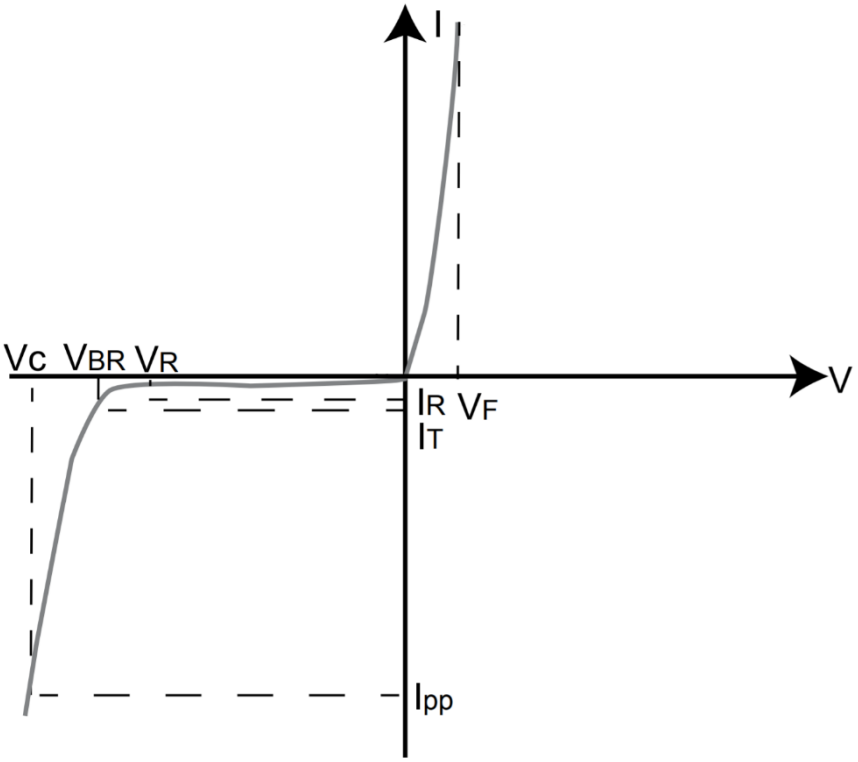

Figure 2.3: Characteristics of a unidirectional TVS diode.

2.5 MOSFETs

A MOSFET is a device that acts like an electronic switch. It has three terminals, the *gate*, *drain* and *source*. There are two basic types, p-channel and n-channel, the difference being in the substrate used on source and drain; p-channel devices use p-type substrate and vice versa. The gate is separated from the body by an insulating layer and by applying a voltage to the gate, a conductive channel is formed between source and drain. In all MOSFETs, there is an intrinsic diode formed in the p-n junction between the body of the device and the drain. The body is usually connected to source (as seen in the schematic symbols), meaning there is a diode between source and drain, and that the MOSFET can only block current reliably in one direction [7].

From datasheets, MOSFETs have the following key electrical characteristics:

- $V_{DS(max)}$ the maximum drain-source voltage V_{DS} without damage to the device.
- $V_{GS(max)}$ the maximum gate-source voltage V_{GS} without damage to the device.
- $R_{DS(on)}$ the resistance between the drain and source when the device is on. It will be a function of V_{GS}.
- I_D the maximum continuous current from drain to source.

The on/off behavior of enchantment mode MOSFETs can be simplified to Table 2.1.

Table 2.1: ON/OFF behavior of enhancement mode MOSFET channel types

	$V_{GS} \ll 0$	$V_{GS} = 0$	$V_{GS} \gg 0$
p-channel	ON	OFF	OFF
n-channel	OFF	OFF	ON

Enhancement mode is the most common. In addition, there are depletion mode MOSFETs, the difference is that depletion modes are normally on at zero V_{GS}. The mode of a MOSFET is usually found by looking at the threshold voltage $V_{GS(th)}$ at which the lowest $R_{DS(on)}$ is achieved.

Since a p-channel MOSFET requires a negative potential on V_{GS} to turn on, they are useful for high side applications since the gate can be readily pulled to ground to turn them on. An n-channel MOSFET requires to be put on the ground side of a load with the gate pulled high to turn on, unless supplemented with extra circuits such as charge pumps to raise V_{GS} above the

supply voltage. Ground side MOSFETs have the disadvantage of raising the ground potential of the load, since there will be a small voltage drop over the MOSFET. This makes them unsuitable for sensitive electronic equipment that rely on a stable ground reference to operate.

The main advantage of an n-channel MOSFET is that physically, the electrons in an n-type substrate have higher mobility than the positive holes in a p-type. This translates to much lower $R_{DS(on)}$, making them desirable in power electronic applications.

Figure 2.4 shows the physical structure of an n-channel MOSFET. Figure 2.5 shows the electrical symbol of enhancement types.

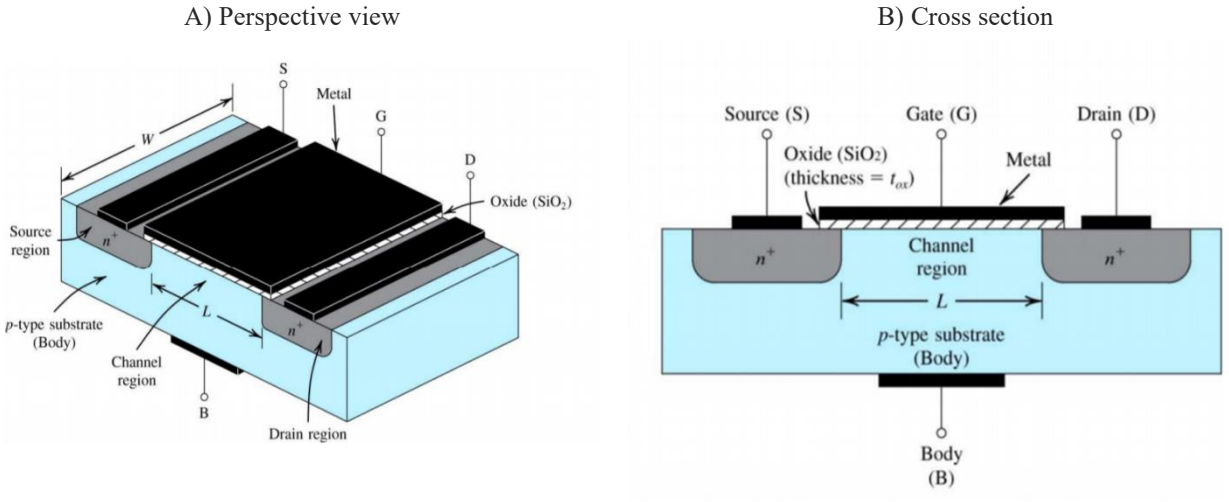

Figure 2.4: Physical structure of a n-channel MOSFET [7].

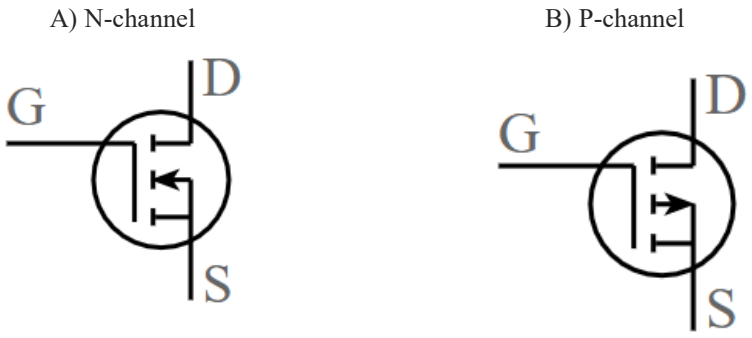

Figure 2.5: Electrical symbol of enchanment type MOSFETs.

Chapter 3
Hardware platform and design

This chapter presents the hardware that was considered, made and used for testing.

3.1 Target specifications

For the purpose of this report, Scout wanted to meet the following specifications:

- Tether length of 30 meters.
- 800 W nominal power during hovering.
- 1500 W peak power consumption.
- 50 Mbit/s real-time data link.
- A safety battery system with automatic switch-over functionality.

3.2 Power quality test platform

Although the end goal was to develop a long-range HV system as described in section 2.2, it was of interest to assess the transient behavior before that system was developed and ready. Therefore, a short-range LV platform was initially used to simulate the low voltage side of air module in the HV system.

The low voltage platform included:

- ~3.5 meter, AWG 12 tether, with ethernet cable.
- 1000 W, 15 V power supply, from MEAN WELL [8].
- Dynamometer from RCbenchmark [9] for single motor benchmarking.
- The drone “Woody” for quad motor benchmarking.

The low voltage platform was initially made and used by Scout before work on this project started, except Woody which was made later. It is shown in Figure 3.2.

The high voltage platform included:

- ~30 meter, 2 x 0.14 mm^2 tether from Helukabel [10].
- 1500 W, 300 V power supply, sourced from seller on eBay [11].
- The developed air power unit (APU) for transforming voltage.
- The drone “Woody” for quad motor benchmarking.

The prototype drones from Scout could not directly be used for testing, since test conditions could damage their equipment. Therefore, as the project developed, a wooden drone “Woody” was made to simulate the powertrain but omitting the payload (see section 2.2) of the final system. It is displayed in Figure 3.1.

Both Woody and the dynamometer were outfitted with 6” propellers, and an XT30 extension plug on the ESC terminals for adding components as seen in Figure 3.1-B.

A) Clamped in place during testing

B) Plug-and-play connector

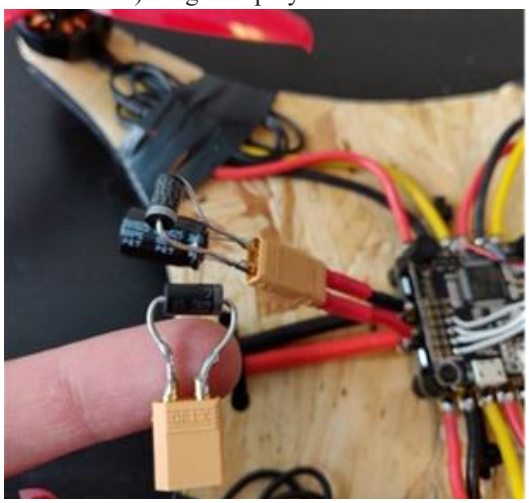

C) Top-down view

Figure 3.1: “Woody” test platform. The ESC and flight controller are stacked in the center.

A) PSU side B) Dynamometer side

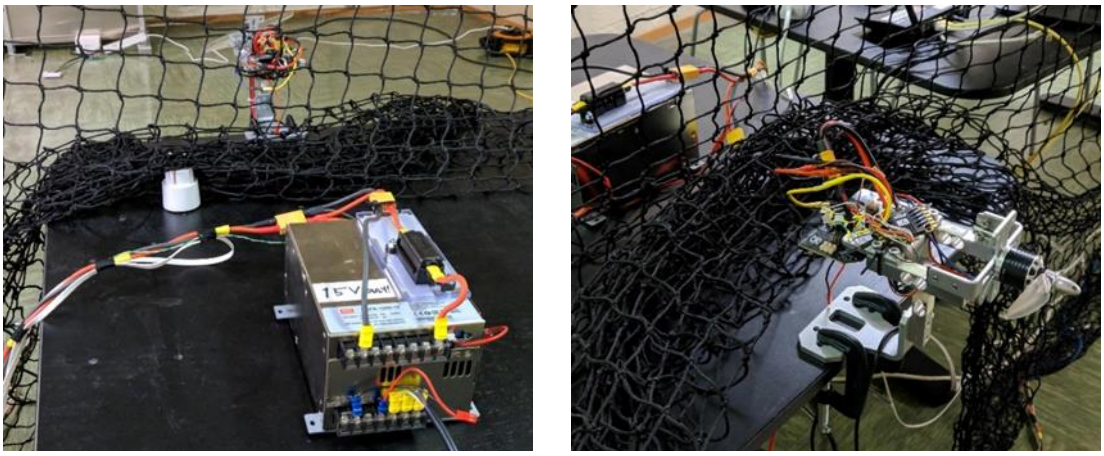

Figure 3.2: Low voltage, single motor test platform.

3.2.1 HV tether and PSU selection

For the tether, Scout had two cables available from Helukabel, one being 0.14 mm^2 and the other 0.25 mm^2. The specifications are listed below, along with an alternative cable that was considered.

Table 3.1: Three cables concidered for the tether.

	Helukabel 0.14 [10]	*Helukabel 0.25* [10]	*igus 0.14* [12]
Copper cross section [mm^2]	0.14	0.25	0.14
Weight [g/m]	22	27	11
Nominal voltage [V]	350	350	300
Jacket material	PUR	PUR	TPE

All the cables are oil and UV resistant, and very flexible. The cable from igus is the lightest, half the weight of the equivalent from Helukabel. However, it was decided to use the Helukabel initially since they were on hand. The lightest (0.14 mm^2) was chosen after testing with voltage drop and heat generation on both (see section 5.1).

For the power supply, the CSP-3000-400 from MEAN WELL [13] was considered ideal, delivering up to 400 V and 3000 W. However, it was not in stock at retailers until late in the development phase. Instead, a 1500 W, 300 V adjustable supply was found on eBay from a factory direct seller that could be delivered within a week [11].

3.3 Air power unit

The air power unit (APU) is the end component of the tether attached to the drone. It is responsible for converting high voltage DC from the ground power supply to a lower voltage usable by the motors and internal drone system.

3.3.1 Component selection

Scout had initially looked at the DC-DC converter modules from Vicor Corporation, a series of devices capable of delivering up to 1750 W and 800 V DC [14].

Vicor claims their products have the highest power density in the industry, and no real alternatives were found. The devices are available in pre-assembled "VIA" packages with input/output terminals, or in chip packages that require a PCB. The chip packages can be made significantly smaller and lighter with a custom PCB and are cheaper, so it was decided to use those.

After some research two systems were proposed:

- Regulated system: 3x DCM4623TD2K17E0T00 (hereby "DCM") [15]
- Unregulated system: 1x BCM6123TD1E2663T00 (hereby "BCM") [16]

Table 3.2 lists the key specifications for each chip.

Table 3.2: Key specifications for the DCM and BCM chips.

	DCM	*BCM*
Continuous power [W]	500	1500
Input voltage V_{PRI} [V]	160 – 420	260 – 410
Output voltage V_{SEC} [V]	15	16.3 – 25.6
Continuous output current I_{SEC} [A]	33.4	62.5
Weight [g]	29.2	41
Retail price [USD]	246	207

The DCM chip is a regulated converter, meaning it can output a constant voltage. The output can be set from 9 to 16.5 V. The BCM chip is unregulated with a constant conversion factor of K = 1/16, i.e. the output is proportional to the input voltage.

Although a constant voltage output would be beneficial with regards to the payload of the UAV, a single chip is only capable of delivering 500 W. Therefore, a minimum of two chips would

be needed in parallel (load sharing) for hovering, and three chips for the peak power consumption of 1500 W. This would add up in weight (87.6 g) and price ($738) when compared to a single BCM chip which weights 41 grams and costs $207. The disadvantage of the BCM chip is naturally that the voltage is unregulated, which necessitates the use of buck converters or other voltage regulators before the payload. The drivetrain and motors, which are powered directly from the APU output, would also need to be designed for the expected voltage range. A 300 V input would equal 18.75 V on the output:

$$(300\,V) \cdot K = (300\,V) \cdot \left(\frac{1}{16}\right) = 18.75\,V$$

Note that, with the 300 V PSU that was chosen and a maximum current output of 62.5 A, the maximum power output of the chip is just short of 1200 W:

$$P = (18.75\,V) \cdot (62.5\,A) = 1172\,W$$

Hence the target specification of 1500 W cannot be met until the PSU is upgraded to 400 V which would output 25 V on the chip.

After thorough discussion with Scout, it was decided to use the unregulated system with a single BCM chip. The official heatsink for this chip was unavailable at all retail stores, so a different one (still from Vicor) was used after confirming the dimensions.

3.3.2 Schematic and PCB design

EasyEDA was used to make the schematic and PCB. It is a web-based, free circuit and PCB design tool [17]. The design was largely based on the reference schematic of the BCM chip's official evaluation board [18].

The final schematic is shown in Figure 3.3.

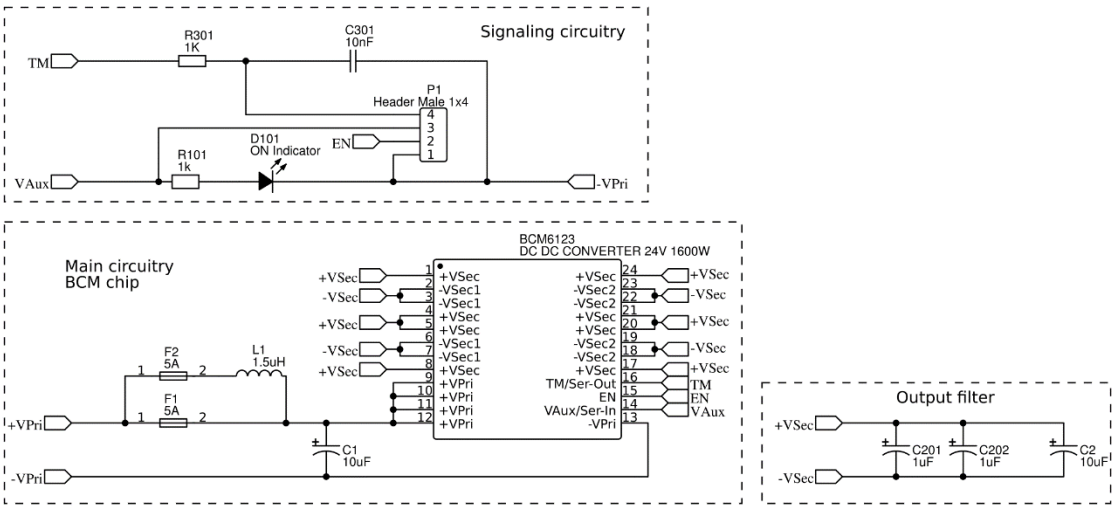

Figure 3.3: Air power unit (APU) final schematic.

The top left section are the signal circuitry. It includes the following:

- TM pin: The internal temperature of the chip is given as a signal with reference to $-V_{PRI}$. R301 and C301 are the recommended low pass filter values, where the output measures 1.27 V at 27 °C and has a gain of 10 mV per °C [16].
- V_{AUX} pin: A fault flag that goes low when an internal fault is detected. It outputs 3.3 V and up to 4 mA when the device is on [16], and is used to drive a green LED, D101, to visualize when the chip is on.
- EN pin: It is internally pulled high when the device is operating and can be pulled low with a jumper to $-V_{PRI}$ which disables the device.

The signals are easily accessed via the header P1 where probes can be attached.

The bottom left section shows the BCM chip and how its pins are connected. The input includes the following:

- C1, a 450 V, 10 µF decoupling capacitor from the reference design [18].
- F1 and F2, where a 5 A, 400 V fast-acting fuse can be installed in either position (exclusively). F2 provides an optional path with L1, a 1.5 µH inductor which makes an LC input filter together with C1.

The bottom right section is an optional output "filter" at V_{SEC} and made up of two small 1 µF decoupling capacitors (C201 and C202) and a larger 10 µF capacitor (C2).

Both L1 and C2 were designed to be swapped with different values, though other values were not used in this report.

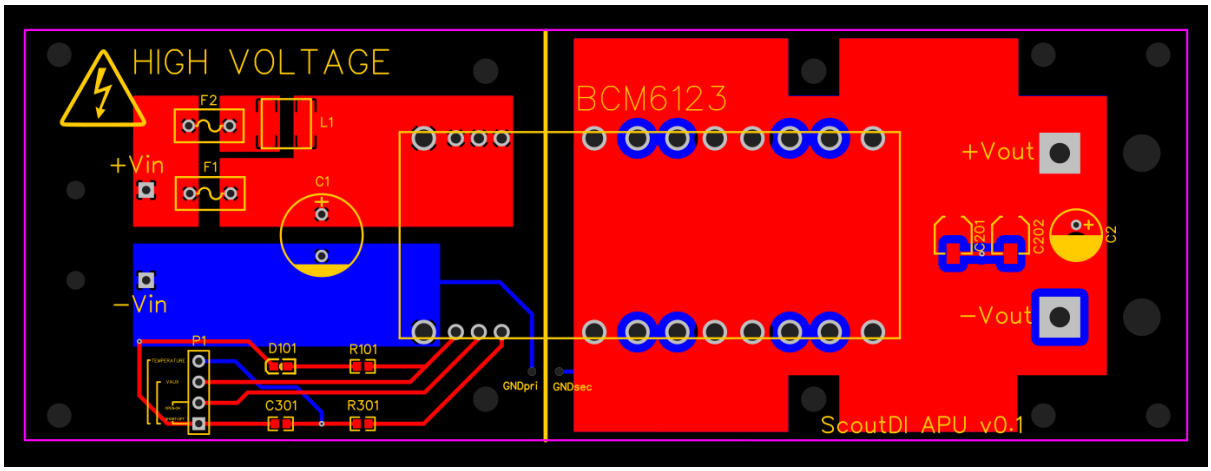

Figure 3.4: PCB layout for the APU.

A) Top layer

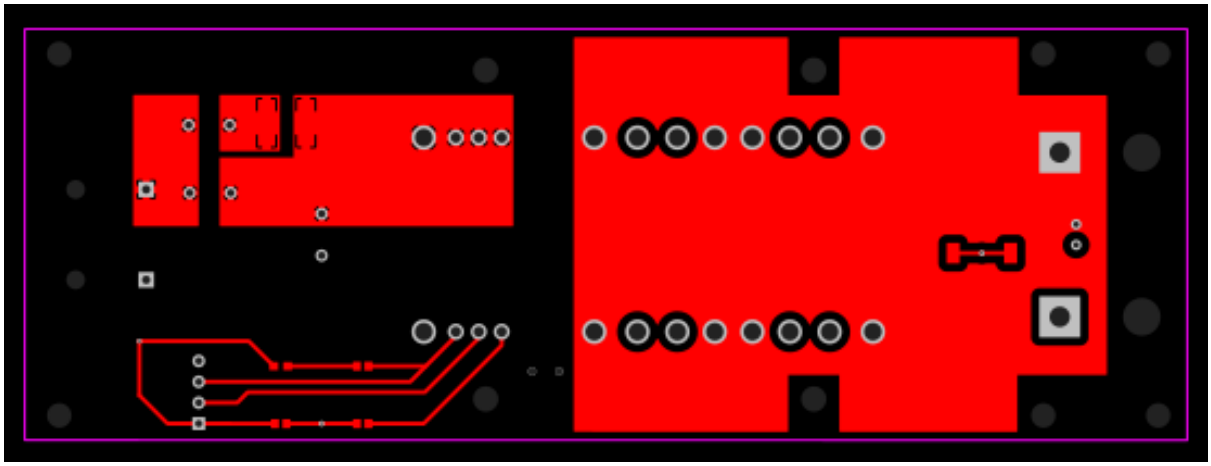

B) Bottom layer

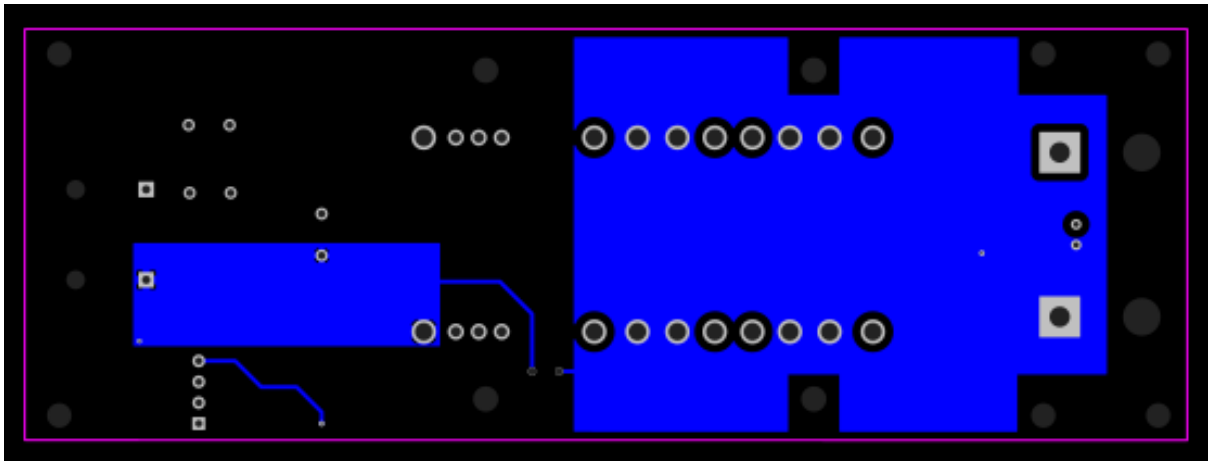

Figure 3.5: PCB top and bottom layers for the APU.

The schematic was then converted to PCB within EasyEDA, and the components routed together with space and current capacity in mind. Figure 3.4 shows the final PCB layout with top and bottom layers as well as the silk screen. Figure 3.5 shows the top and bottom layers separately.

The purple line is the outline with dimensions 142 mm x 50 mm. The top layer is red, bottom layer blue and the silk screen yellow.

The high side, $+V_{PRI}$ and $+V_{SEC}$ were both routed on the top layer. Likewise, the ground side, $-V_{PRI}$ and $-V_{SEC}$ were routed on the bottom layer. Copper pouring was used on the paths carrying the main current, with a weight of 2 oz/ft^2. The secondary side used the entire width of the PCB to distribute current and heat. Using an online copper width calculator [19], with 62.5 A, an ambient temperate of 25 °C and temperate rise of 50 °C, the required trace width should be 44.1 mm, which is satisfied.

In addition to the components, pads were added for the input and output conductors, with additional holes to relieve mechanical stress. Holes were also put in the corners for mounting to the drone, and around the heatsink, though these were designed for the correct heatsink and not the one that was used. Ground pads were also added on both the primary and secondary side to ground the heatsink (secondary was used).

Finally, the PCB gerber file was generated and ordered directly through EasyEDA with their sister company, JLCPCB, together with the components (except BCM chip). The PCB is shown in Figure 3.6.

Figure 3.6: Final, physical PCB for the APU.

3.3.3 Final assembly

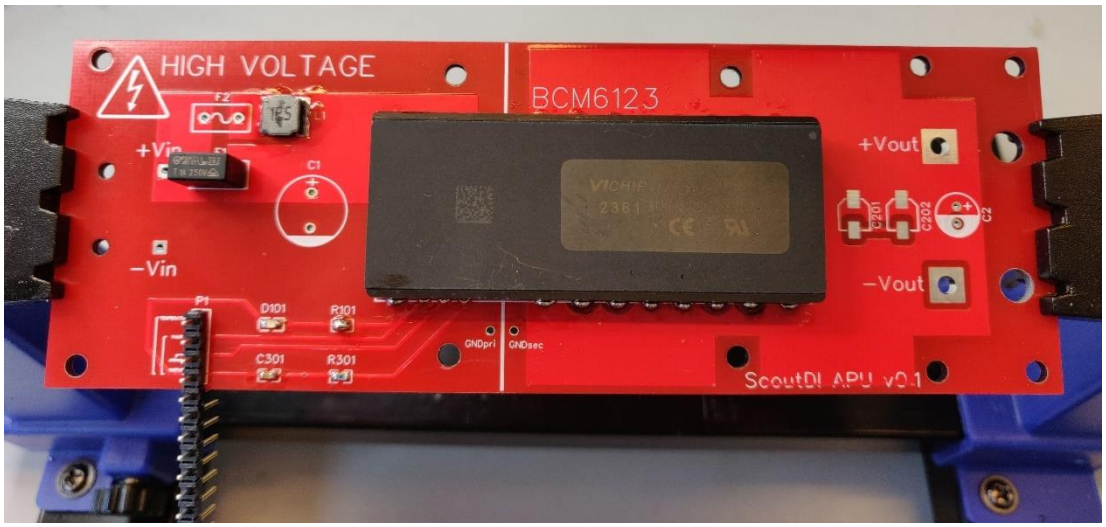

Figure 3.7: APU during assembly process.

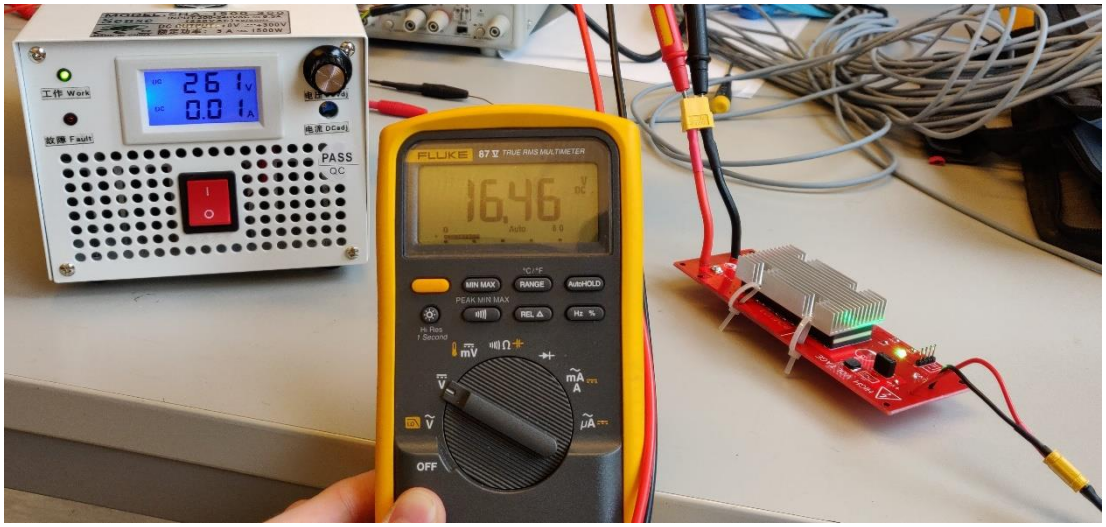

Figure 3.8: Functional APU showing voltage transformation.

Figure 3.7 shows the BCM chip soldered onto the PCB. Figure 3.8 shows the PSU at 261 V, connected to the APU input through the tether and measuring 16.46 V on the output. This corresponds well to the conversion ratio of 1/16.

The APU weighed a total of 112 grams, less than Vicor's VIA package which weighs 140.5 g [14]. Additional weight could potentially be saved without the extra circuit elements made for experiments and monitoring (filters, temperature etc).

3.4 Battery backup interface

The simplest form of adding power redundancy or load sharing to a system is the passive diode ORing circuit, see Figure 3.9.

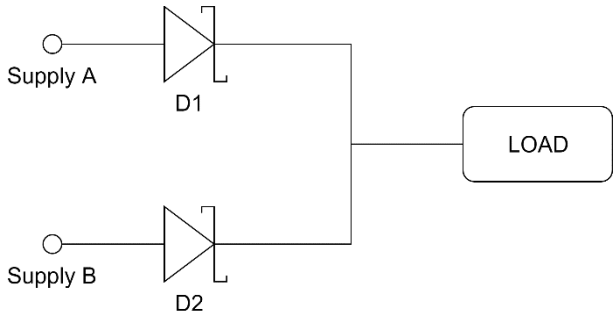

Figure 3.9: Diode ORing circuit.

If the diodes have the same forward voltage drop V_f, then whichever source supply is higher will power the load. This is easiest seen by example:

$$Let \quad V_A = 3\,V, \quad V_B = 2.9\,V, \quad V_f = 0.7\,V$$

$$V_{load} = V_A - V_f = 2.3\,V$$
$$V_{D2} = V_B - V_{load} = 0.6\,V$$

But since $V_{D2} < V_f$ the diode cannot turn on, leaving Supply A alone to power the load.

The advantage of this circuit is its simplicity. The major disadvantage is the voltage drop at the diodes resulting in power loss. Better efficiency can usually be achieved by incorporating MOSFETs as “ideal diodes”, which exhibit very low on-state resistance and thus a lower power loss.

The following sections present the two main iterations of the backup battery interface.

3.4.1 Passive circuit

The first battery switch interface that was developed was a passive circuit, see Figure 3.10. It differs from the diode ORing circuit in that it incorporates a MOSFET.

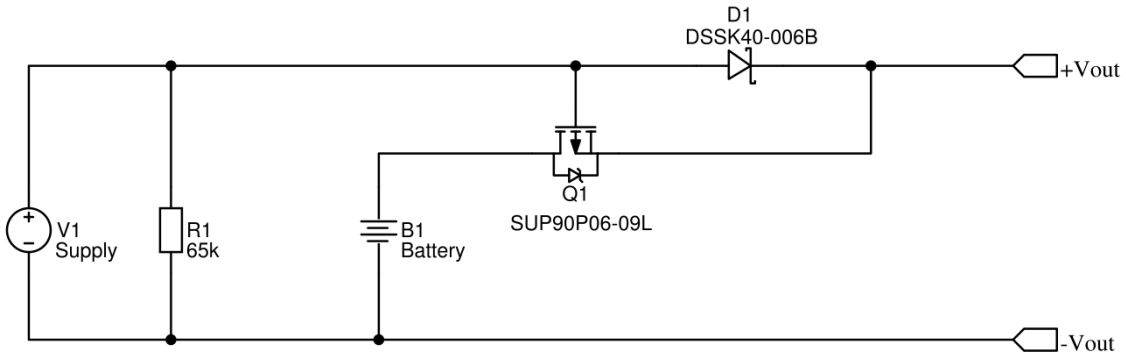

Figure 3.10: Passive backup battery interace.

In the circuit, V1 is the supply voltage, B1 is the backup battery, R1 is a high ohmic resistor, D1 are two Schottky diodes in parallel [20] and Q1 are two p-channel MOSFETs in parallel [21]. For simplicity, Figure 3.10 shows D1 and Q1 as a single component.

The circuit works like this:

- When the supply is on, the gate of Q1 is high and the MOSFET turned off.
  - Current flows from the supply to the output via D1. Q1 is off ensuring no current flows into the battery.
- When the supply is off, the body diode of the MOSFET starts conducting briefly.
  - The gate of Q1 is pulled low via R1 and the gate-source voltage goes low $V_{GS} = 0 - (\mathrm{V_{OUT}})$, turning the MOSFET on.
  - Current flows from the battery to the output via Q1. D1 blocks current from flowing into the supply.

Unlike the diode ORing circuit, this circuit has the immediate advantage of using a MOSFET in the backup supply path. This means less power is wasted as heat when operating on battery, increasing flight time. The tether has an infinite power source and thus power loss is less important, though the heat still needs to be dissipated.

It is recommended to always keep the supply voltage higher than the battery as a rule, since the body diode of the MOSFET will be very inefficient if turned on.

Component dimensioning were done at 25 V and 60 A (approximately APU output limit), and an ambient temperature T_A of 25 °C.

R1 is a generic 65 kΩ, ¼ W resistor. It would dissipate 9.62 mW which is negligible.

Q1 has an $R_{DS(on)}$ of 9.3 mΩ and continuous current draw I_D of 90 A. At 60 amps, a single device would dissipate

$$P = (60\ A)^2 \cdot 9.3\ m\Omega = 33.5\ W$$

which is quite high. Two devices in parallel share the current and thus the power dissipation per device will be 8.4 W (25 %) and the total losses to 16.8 W (50 %).

The maximum allowed junction temperature $T_{J(max)}$ is 175 °C, and junction-to-case resistance R_{thJC} is 0.6 °C/W. The heat sink (and thermal interface) would then need a minimum sink-to-air resistance R_{thSA} of about 17.3 °C/W:

$$\begin{aligned} T_{J(max)} &> T_A + P \cdot R_{th} \\ 175\ °C &> 25\ °C + 8.4\ W \cdot (0.6 + R_{thSA})\ °C/W \\ R_{thSA} &< 17.3\ °C/W \end{aligned}$$

D1 has a very low V_f of 0.5 V, but a maximum current of 40 A, hence the need for two devices. The dissipation per element is then

$$P = 0.5\ V \cdot 30\ A = 15\ W$$

and the total losses 30 W. Note that paralleling diodes does not inherently reduce the total losses like with MOSFETs, since the voltage drop is constant.

This device has a $T_{J(max)}$ of 150 °C and R_{thJC} of 1.1 °C/W, so the heatsink would need to be at least 7.23 °C/W. The assembled (clunky) circuit is shown in Figure 3.11.

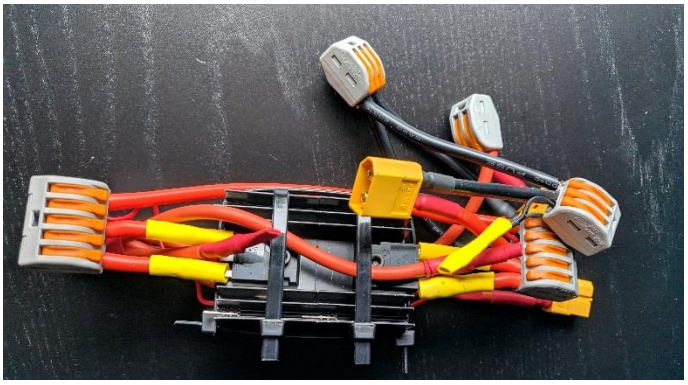

Figure 3.11: The passive battery backup interface prototype.
The diodes are visible on the front, the MOSFETs are on the backside of the heatsinks.

3.4.2 Active circuit

The active circuit is a variant of the diode ORing circuit with “ideal diodes”; n-channel MOSFETs and an IC chip to control them, see Figure 3.12.

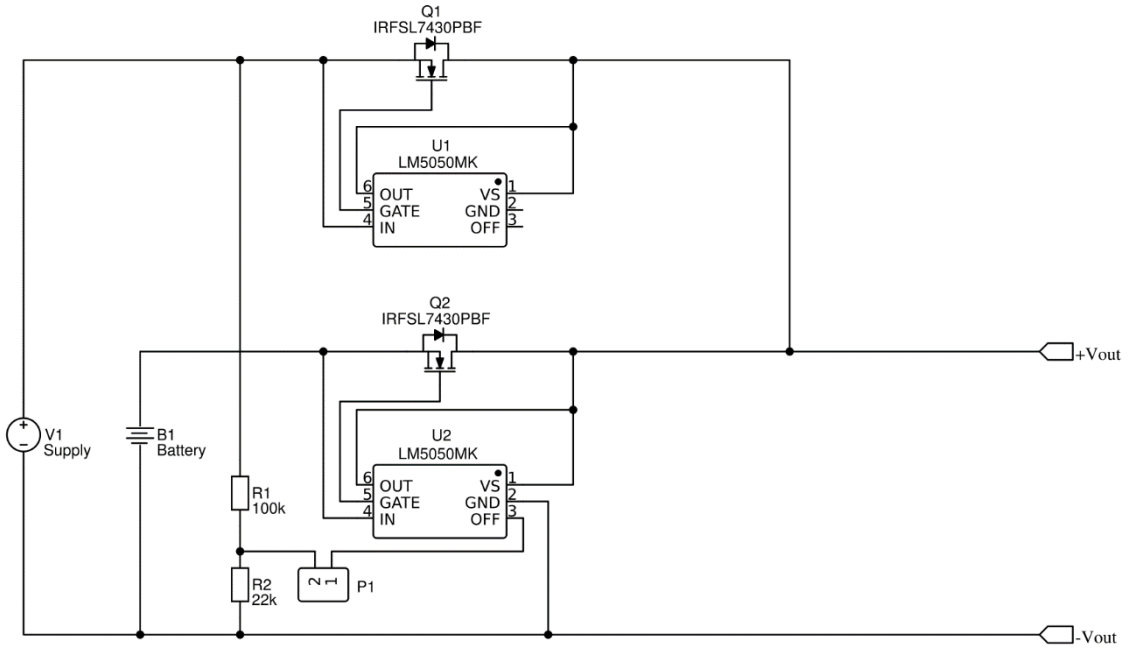

Figure 3.12: Active backup battery interace.

V1 is the supply voltage and B1 is the backup battery. Like the diode ORing circuit, whichever source is higher will power the load and V1 should be set higher than B1.

Q1 and Q2 are n-channel MOSFETs [22]. U1 and U2 are ICs [23] that control the FETs like diodes by pulling the gate high with a charge pump when the input is greater than the output. They operate from 1 to 75 V and can turn off very fast (50 ns). Since the MOSFETs act like diodes, an added benefit of this circuit is that is provides reverse polarity protection.

The OFF pin on U2 is a logic gate and is left as an option that can force Q2 off if V1 is high. The pin operates up to 5.5 V and the resistors R1 (100 kΩ) and R2 (22 kΩ) make a voltage divider at 4.5 V if the supply is 25 V. The jumper on P1 can be used to activate this function, though it was left disconnected during testing.

Q1 and Q2 have a very low $R_{DS(on)}$ of 0.97 mΩ and I_D of 195 A. At 60 A they would dissipate only 3.5 W:

$$P = (60\ A)^2 \cdot 0.97\ m\Omega = 3.5\ W$$

With a $T_{J(max)}$ of 175 °C and junction-to-ambient resistance R_{thJA} of 40 °C/W, a heat sink is in theory not needed (but used in practice):

$$T_J = 25\,°C + 3.5\,W\ \cdot 40\,°C/W = 165\,°C$$

R_{thJC} is 0.4 °C/W and the heat sink's R_{thSA} is 16.6 °C/W, so a junction temperature of 84.5 °C is expected at full load 60 A.

The circuit was soldered on a prototype board, seen in Figure 3.13.

A) Front side

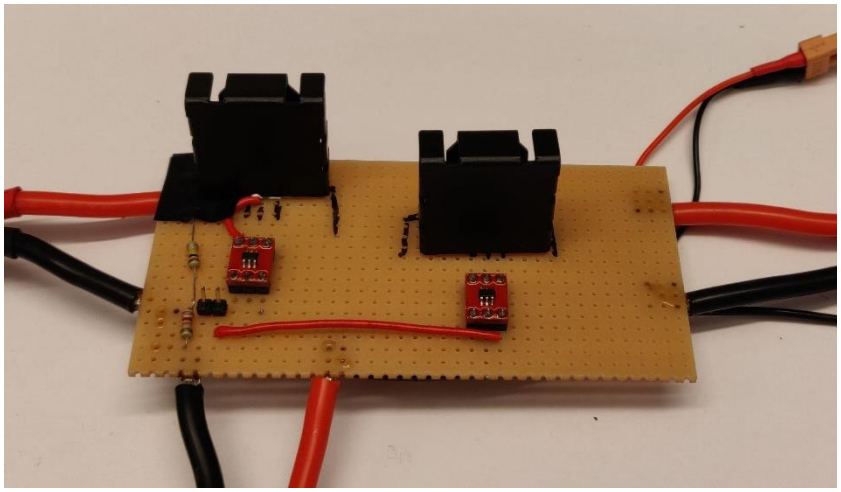

B) Back side

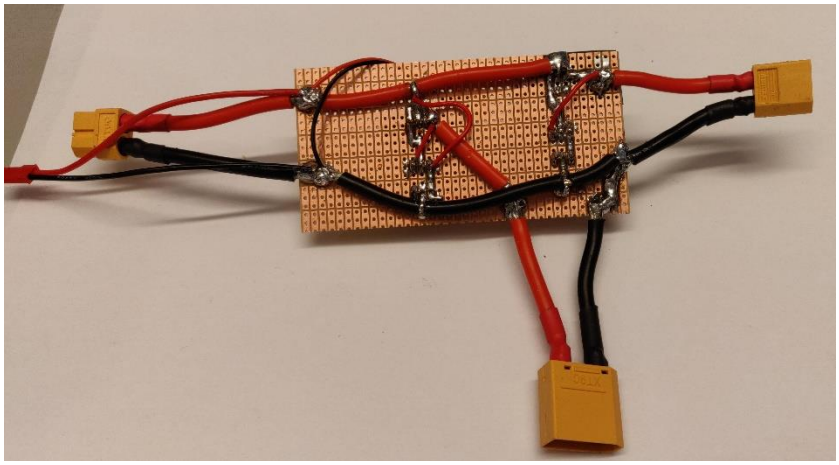

Figure 3.13: The active backup battery interface prototype.
In B), the output connector is on the left, supply input on the right and battery input at the bottom.

3.5 Data link

The data link between the drone and ground was established using the LX200V20 [24] module from Rak wireless and the WisPLC development board [25].

This is a relatively small and lightweight module capable of up to 200 Mbit/s over power lines up to 300 m, using differential signaling. The WisPLC board provides an interface for RJ-45 plugs, micro-USB, power supply and the power lines, see Figure 3.14.

The only modification needed for this device was to exchange C9 and C11 at the signal interface with capacitors rated for 1000 V (0.01 uF) to allow a 2x headroom on the tether (which was 300 V, scalable to 400 V), see Figure 3.15.

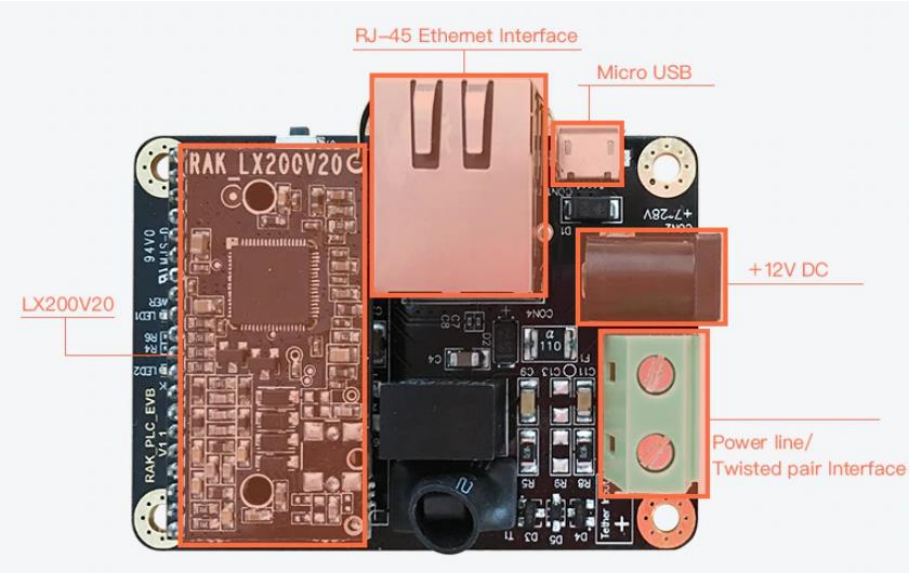

Figure 3.14 WisPLC development board overview [25].

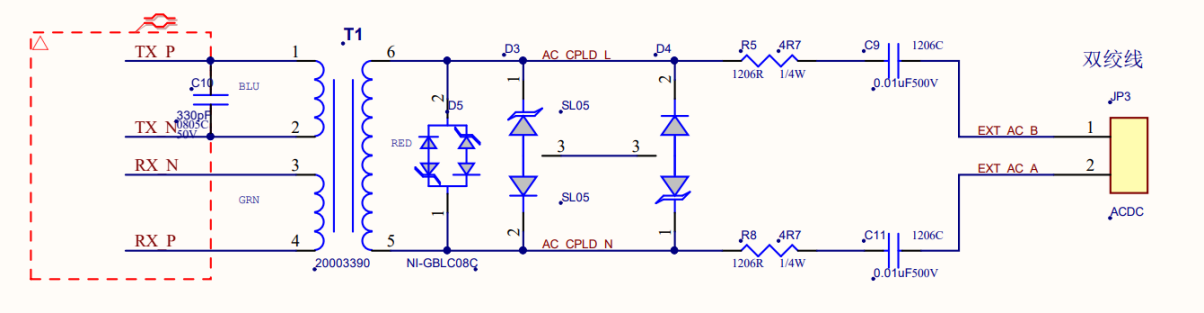

Figure 3.15: Differential signal connector schematic from the WisPLC board [25].
C9 and C11 was upgraded to 1000 V.

To establish the data link between the ground and the drone, two modules needed to be used, one on each end of the tether. The ground side module was powered by an adapter while the drone side module could be powered by adapter or directly from the APU output when flying.

The differential signal was connected directly onto a split from the tether on each conductor. Initially the boards were tested directly onto the power line, but differential mode chokes were later made by wiring the conductors over a ferrite core, see Figure 3.16. The chokes were installed as seen in Figure 3.17.

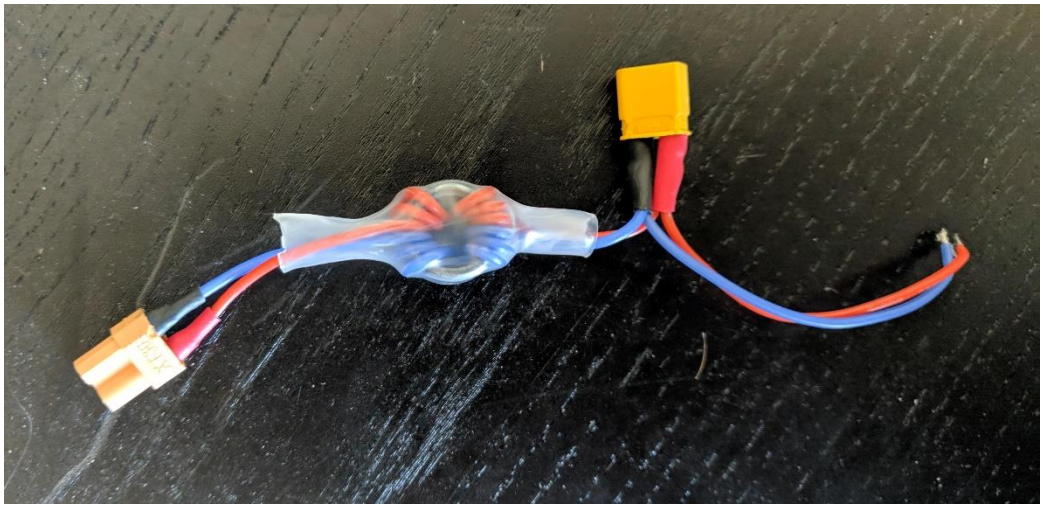

Figure 3.16: A differential mode choke, used on both ends of the tether.

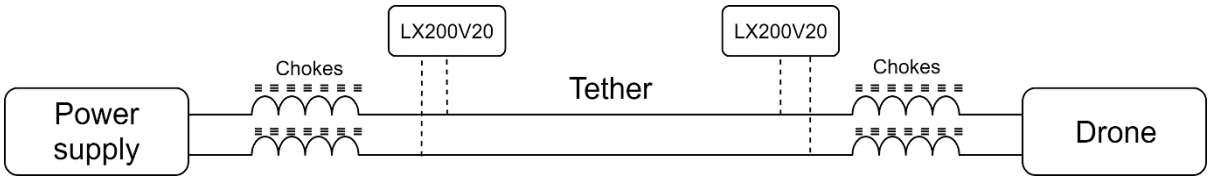

Figure 3.17: Configuarion for adding chokes on the tether.

Chapter 4

Low voltage system power quality

This chapter shows results related to the power quality of the low voltage system.

4.1 Measuring transients

An oscilloscope [26] was used to measure transient voltage close to the terminals of the ESC with a probe.

Transient current was measured at the points of interest with the scope using a sensor with conversion factor 30.6 A/V [27]. Steady state current (before disarming) could not be reliably read with the sensor and was instead read directly from either the software or the PSU if available.

The motors were controlled on the dynamometer using the software utility from RCbenchmark [9], and on Woody using the Betaflight software [28].

To measure transients, the motors were run at intervals of 20% of thrust and then disarmed to simulate a power cut. Some measurements were left out to speed up testing on the following reasoning:

i) From 0 to 40 % thrust, the current draw is small and thus the transient too small for a voltage suppressor to show an effect.
ii) On 100 % thrust the power consumption is unrealistically high, for example on a single 1700 Kv motor up to 460 W (per motor!), while the target total power consumption on four motors is closer to 800 W hovering and 1500 W peak.
iii) With four motors the PSU could turn off before reaching 100 % thrust, making the measurement impossible.

4.1.1 How to read plots

Plots are limited to screenshots, since digital export is not supported on this oscilloscope. This means axes are not readily available.

Divisions are defined with a specific interval for each figure. “5 V/div” means each division (on the y-axis) has a difference of 5 volts. The zero reference is by default in the center, though an offset is usually set and is defined in the legend given for each figure. “ofs -10 V” means the offset is -10 volts, i.e. if the y-axis is 5 V/div, then the reference is two divisions below the center line.

On the bottom of the plots, some quantities such as maximum and mean values are automatically measured by the scope. The respective probe or channel is shown on the left, followed by the type of measurement and its local value. The global maximum and minimum values on the right are sometimes erroneous and can be ignored.

See Figure 4.1 as an example.

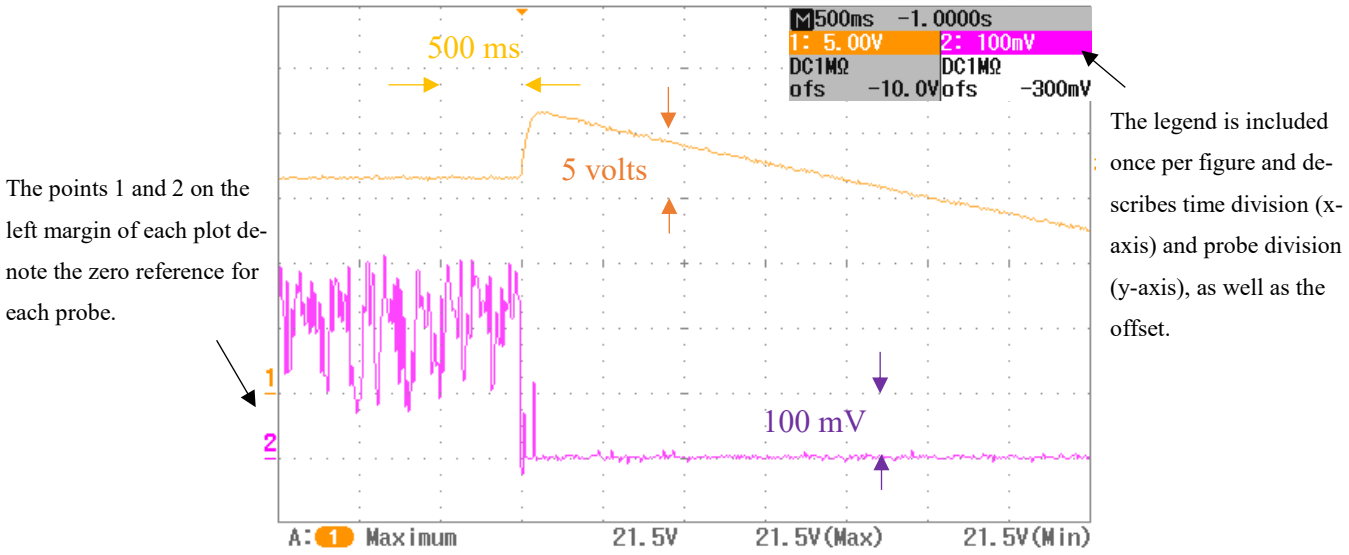

Figure 4.1: Example plot and how to interpret the axes.

X-axis: Time [500 ms/div]. Y-axis: Voltage in yellow [5 V/div], current in purple [3.1 A/div].

The figure description will always state the current in amperes per division. In this example the current is 3.1 A/div:

$$\left(100\ \frac{mV}{div}\right) \cdot \left(30.6\ \frac{A}{V}\right) \approx 3.1\ \frac{A}{div}$$

4.2 Low voltage response part 1 (16.5 V)

This section shows transient response results from 16.5 V supply on 780 and 1700 Kv motors.

4.2.1 Single 780 Kv motor baseline

The baseline measurements on 16.5 V supply voltage and a single 780 Kv motor are shown in Table 4.1 and the Figure 4.2 below.

Table 4.1: Baseline values measured on 16.5 V / single 780 Kv.

Thrust	*Current [A]*	*Power [W]*	*Peak voltage [V]*	*Rise time [ms]*
20 %	0.1	2	16.8	52
40 %	1	17	18.1	72
60 %	3.1	52	20	72
80 %	6.5	106	21.5	92
100 %	9.5	157	22.8	104

Current and power denote the steady state consumption before triggering the disarm, and rise time is the time period from disarming until the peak voltage is reached.

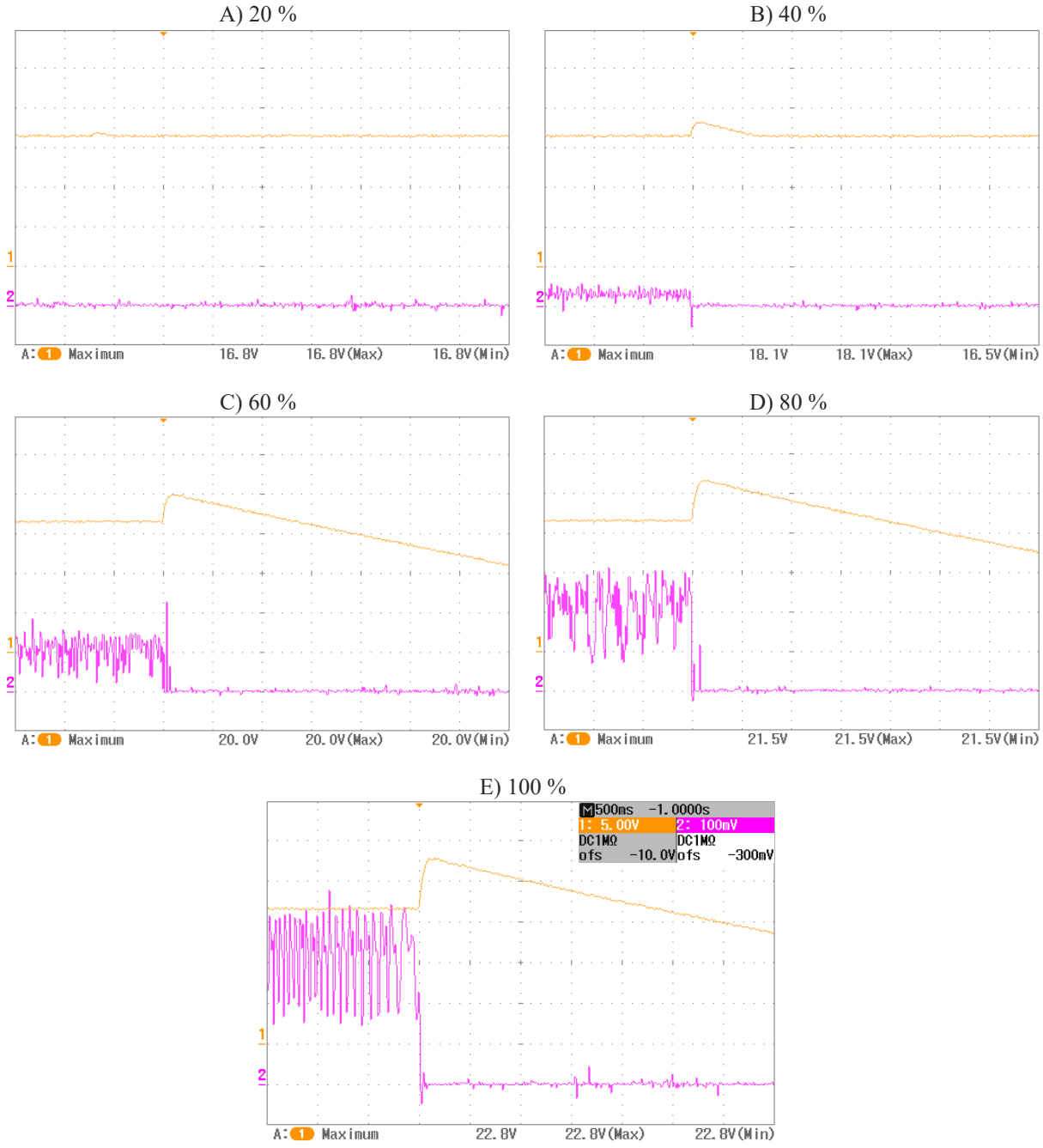

Figure 4.2: Baseline response on 16.5 V / single 780 Kv.

X-axis: Time [500 ms/div]. Y-axis: Voltage in yellow [5 V/div], current in purple [3.1 A/div].

The voltage starts rising when the motor is disarmed. The voltage peak and rise time increase with power consumption, though at 20 % this is barely noticeable, likely due to the low power consumption. From 40 to 100 %, The current drops to zero almost immediately, and some reverse current can be observed. Somewhere between 40 and 60 %, the peak causes the power supply to shut down, as seen in 60 % and above where the voltage keeps dropping below the nominal level.

4.2.2 Single 780 Kv motor with a series diode

A diode in series with the ESC yielded the following plot at 60 % thrust.

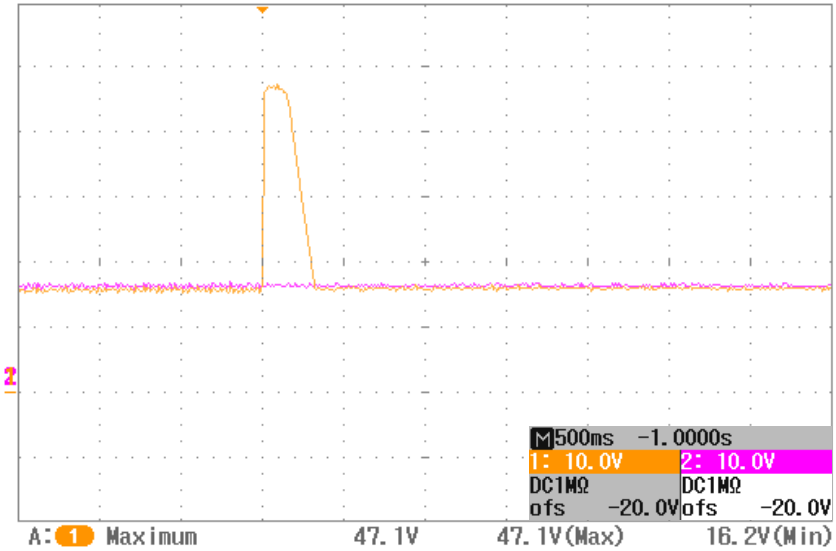

Figure 4.3: Series diode response at 60% thrust.

X-axis: Time [500 ms/div]. Y-axis: ESC in yellow [10 V/div], PSU in purple [10 V/div].

The diode prevents a rise on the PSU side as shown in purple, and thus the supply from shutting down. However, the drone side voltage now peaks at 47.1 V, compared to the baseline of 20 V, and thus not recommended to use.

4.2.3 Single vs quad 780 Kv motor

Before Woody was available, a comparison between single and quad motors was made. A drone from Scout with four motors was connected to the low voltage tether with all sensitive electronics disconnected and held in place physically. The PSU output current was monitored before disarming, such that the same motor on the dynamometer could be tested consuming about 1/4 of the total current draw. The result is shown in Figure 4.4.

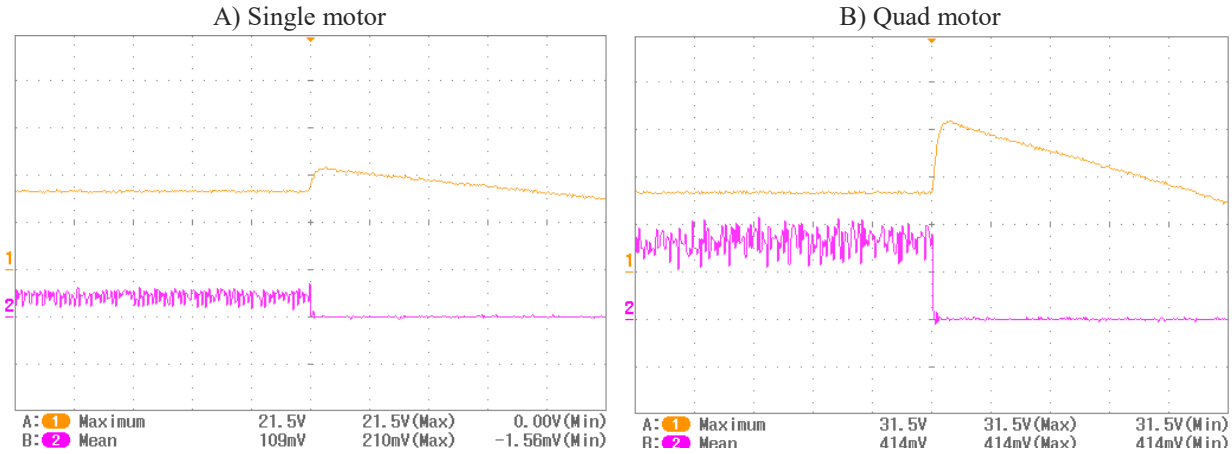

Figure 4.4: Single motor on dynamometer vs. quad motor on drone response.
X-axis: Time [500 ms/div]. Y-axis: Voltage in yellow [10 V/div], current in purple [15.3 A/div].

Based on the mean current measured in plot A (averaging the right half part to zero), the single motor power draw can be approximated to about 6.7 A or 111 W:

$$(2 \cdot 0.109\,V) \cdot \left(30.6\,\frac{A}{V}\right) \approx 6.7\,A$$

$$6.7\,A \cdot 16.5\,V \approx 111\,W$$

Similarly, the quad motors in plot B consumed on average about 25.3 A or 417 W, i.e. each motor consumed ~104 W.

With a nominal voltage of 16.5 V, the single motor peaks at 21.5 V or $\Delta V = 5$ V, while the quad motors peak at 31.5 V or $\Delta V = 15$ V, three times higher than the single motor. Considering the slightly higher individual power consumption on the single motor, the relationship between voltage rise and the number of motors is resembling a linear one.

4.2.4 Single 1700 Kv motor baseline

The single 1700 Kv motor and 16.5 V supply voltage was one of the most extensively tested configurations, including baseline, TVS diodes and capacitors.

The baseline measurements on 16.5 V supply voltage and a single 1700 Kv motor are shown in Table 4.2 and Figure 4.5 below.

Table 4.2: Key values measured on 16.5 V / single 1700 Kv.

Thrust	*Current [A]*	*Power [W]*	*Peak voltage [V]*	*Rise time [ms]*
20 %	0.6	10	17.1	24
40 %	3.4	56	18.9	36
60 %	10.4	172	21.1	90
80 %	19.3	318	23.7	98
100 %	28.1	464	23.4	98

Similar results are observed when compared to the 780 Kv motor. The voltage peak and rise time stays about the same, despite the current draw being about three times higher on the 1700 Kv motor. Again, the power supply shuts down somewhere between 40 and 60 %. The voltage is also characterized by more ripples in the steady state and in the transient rise as seen in plots C and D. This is likely due to the higher current draw and speed of the motor.

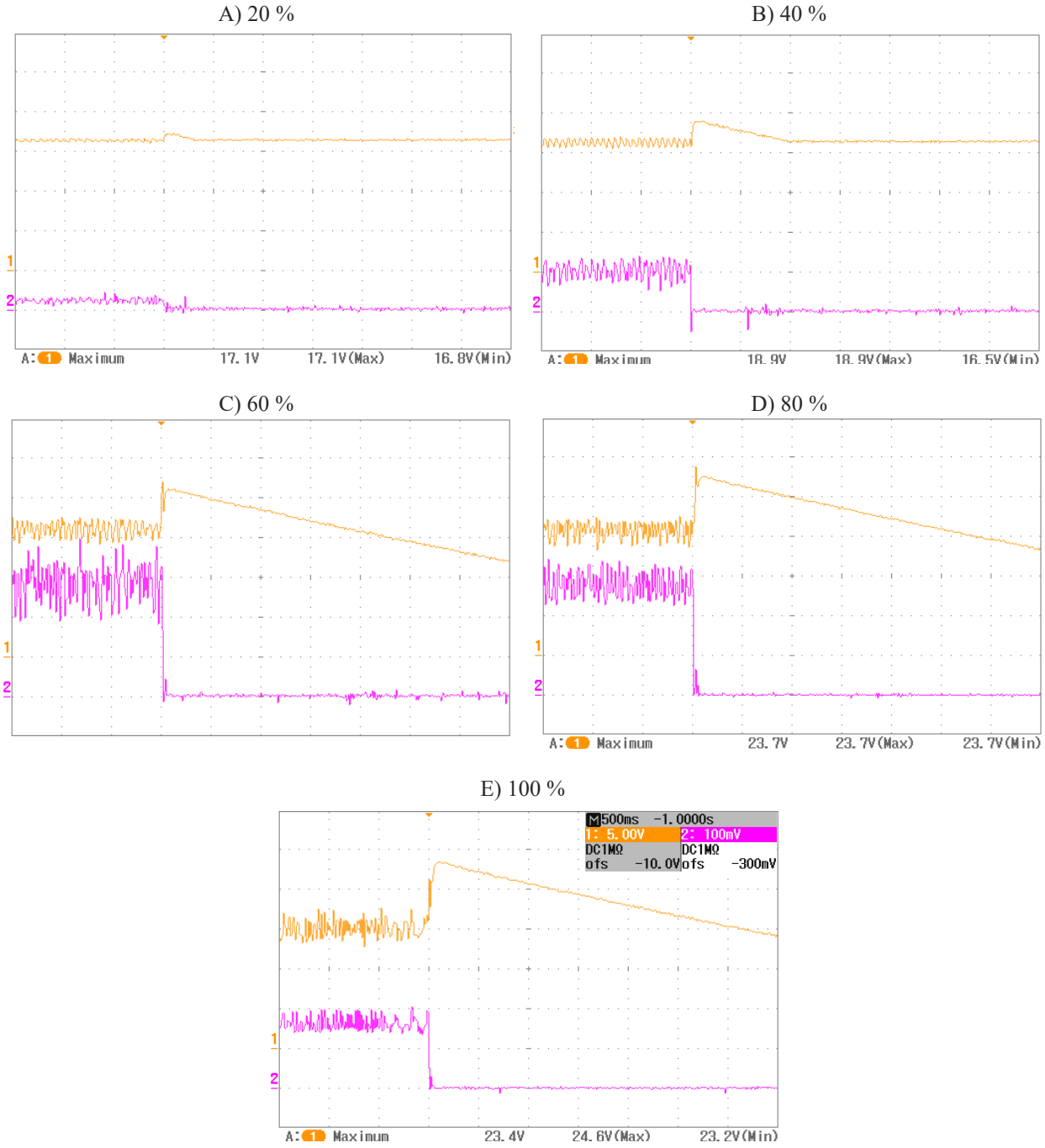

Figure 4.5: Baseline response on 16.5 V / single 1700 Kv. The maximum voltage in C is 21.1 V. X-axis: Time [500 ms/div]. Y-axis: Voltage in yellow [5 V/div], current in purple [3.1 A/div].

4.2.5 Single 1700 Kv motor with components

The components were soldered to an XT30 plug and attached to the ESC. They are displayed in Figure 4.6 with specifications listed in Table 4.3.

Figure 4.6: Example of components made for testing. They included single TVS diodes, capacitors and combinations of them in parallel.

Table 4.3: Specifications of selected TVS diodes.

	16 V	*18 V*	*20 V LF*	*20 V ON*
Manufacturer	Taiwan Semiconductor	ST Microelectronics	Littelfuse	ON Semiconductor
Part number	1.5KE16A	1.5KE18A	1.5KE20A	1.5KE20AG
I_{PP} *[A]*	70	59.5	54.9	54
P_{PP} *[W]*	1500	1500	1500	1500

All the diodes are axial through-hole components (THT). The nominal breakdown voltage is given by the part number and the table entry, e.g. “20 V LF” has a nominal breakdown voltage of 20 V. I_{PP} denotes the maximum peak pulse current and P_{PP} the maximum peak power dissipation.

The capacitors used in this section are low ESR and rated at 35 V.

Table 4.4 shows measured peak voltages at baseline and a selection of components.

Table 4.4: Peak voltages in volts [V] for different diodes and capacitors on 16.5 V / single 1700 Kv.

Thrust	*Baseline*	*TVS 18 V*	*TVS 20 V LF*	*TVS 20 V ON*	*470 uF*	*1000 uF*	*TVS 18 V + 470 uF*
20 %	17.1	17.1	17.1	17.1	n/a	n/a	n/a
40 %	18.9	18.1	18.9	19.8	n/a	n/a	18.4
60 %	21.1	18.4	20.0	21.0	20.9	20.9	18.7
80 %	23.7	19.2	20.3	20.7	22.6	22.3	18.4
100 %	23.4	18.5	n/a	n/a	n/a	n/a	n/a

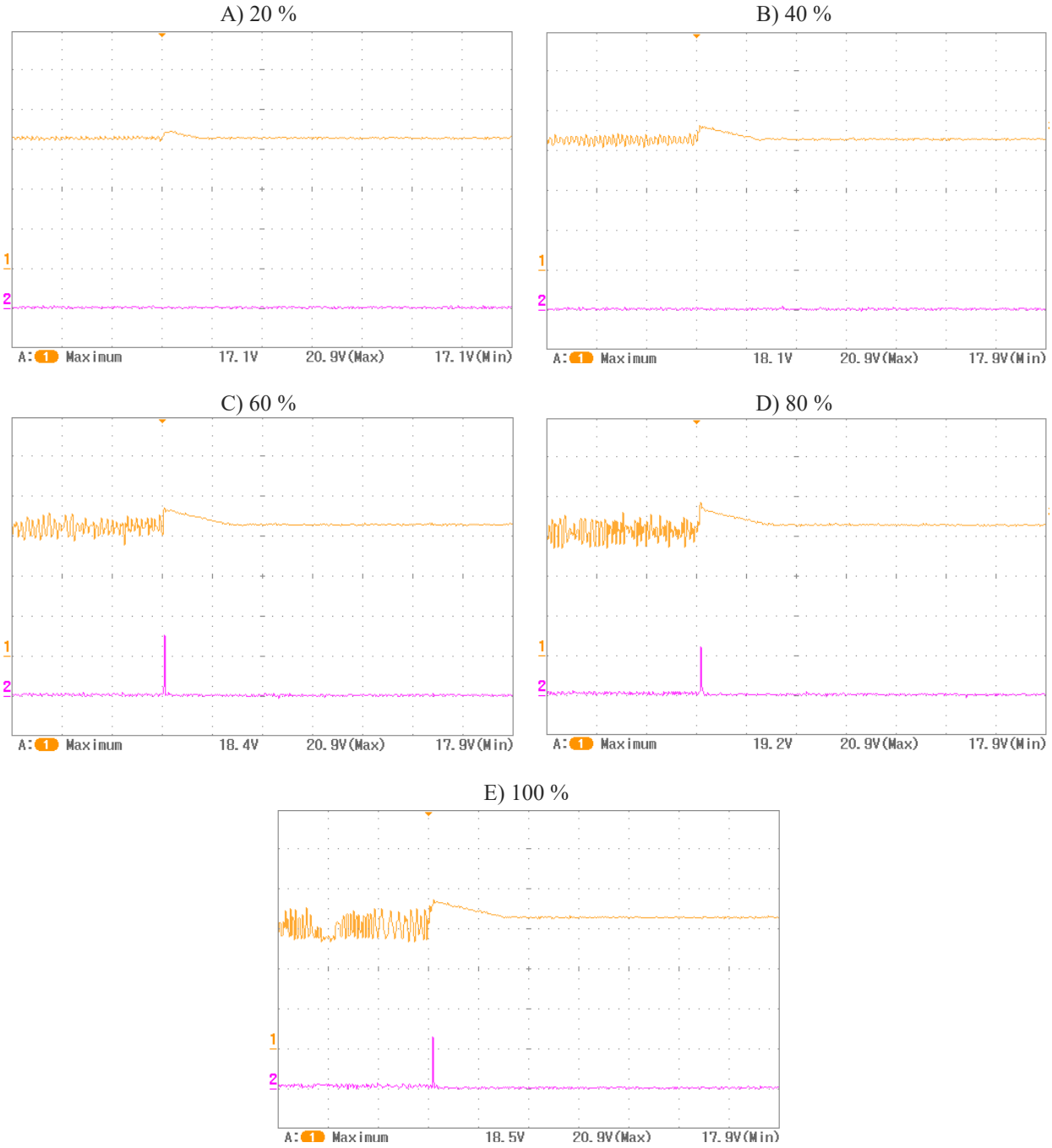

Figure 4.7: Response from an 18 V TVS on 16.5 V / single 1700 Kv.

X-axis: Time [500 ms/div]. Y-axis: Voltage in yellow [5 V/div], diode current in purple [15.3 A/div].

Figure 4.7 shows the results from the 18 V TVS diode in parallel. Current flow through the diode is shown in purple. No significant current was absorbed at 20 or 40 % thrust. At 60 % the current appears to peak as high as 23 A if the peak is read at 750 mV:

$$(750\ mV) \cdot \left(30.6\ \frac{A}{V}\right) = 23\ A$$

This might be an error or a very short fluctuation, since the average draw at 60 % is only 10.4 A (Table 4.2). 80 and 100 % both suggest about 625 mV or 19.1 A which corresponds very well to 80 %, but less than 100 %. Some of that energy might have dissipated somewhere else.

In plot D at 80 %, it is seen that the voltage peaks very fast, then falls steeply during the small interval where the diode is turned on (current spike), then declines at a slower rate again after the diode shuts off.

Most importantly, the diode successfully prevents the PSU from shutting down in all cases.

On the 20 V diodes, it would seem the diode from ON Semiconductor is worse than the one from Littelfuse, though the test on this diode was prone to more ripples during the transient as seen in Figure 4.8-A. Both diodes do not prevent the PSU from shutting down, as the voltage is seen to continue dropping past the supply voltage. Thus the 18 V diode is the only satisfactory solution. It should be noted, compared to baseline which reached 23.7 V, all the diodes show an improvement with the highest recorded voltage being 21 V.

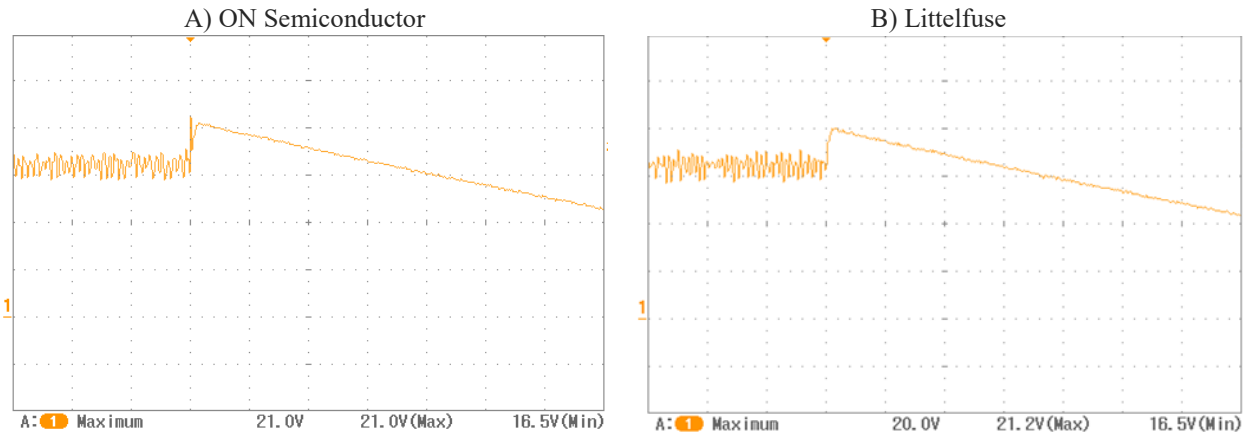

Figure 4.8: Response from two different 20 V TVS diodes at 60 % thrust on 16.5 V / single 1700 Kv. X-axis: Time [500 ms/div]. Y-axis: Voltage [5 V/div].

Results from the capacitors rated 470 uF and 1000 uF are shown in Figure 4.9.

A) 470 uF at 60 %

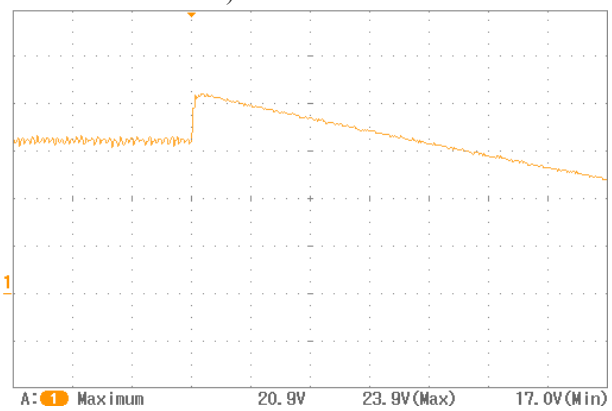

B) 1000 uF at 60 %

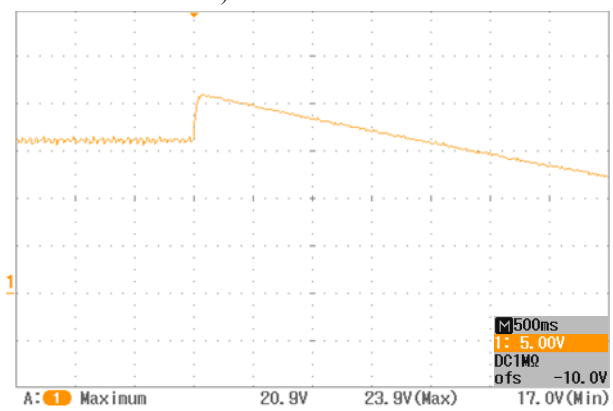

Figure 4.9: Response from 470 uF and 1000 uF capacitors at 60 % on 16.5 V / single 1700 Kv.
X-axis: Time [500 ms/div]. Y-axis: Voltage [5 V/div].

Unlike the TVS diodes which only clamps overvoltage, the capacitors have two functions. Firstly, they reduce the peak somewhat down to 22.6 V in the worst case, but still not in a satisfactory manner since they do not prevent the PSU from shutting down. More importantly however, they reduce the voltage ripples and noise significantly. The 1000 uF capacitor is slightly better, but not by much.

A smaller rated capacitor takes up less space and weight. Figure 4.10 shows results from 1000 uF down to 10 uF at 80 % thrust.

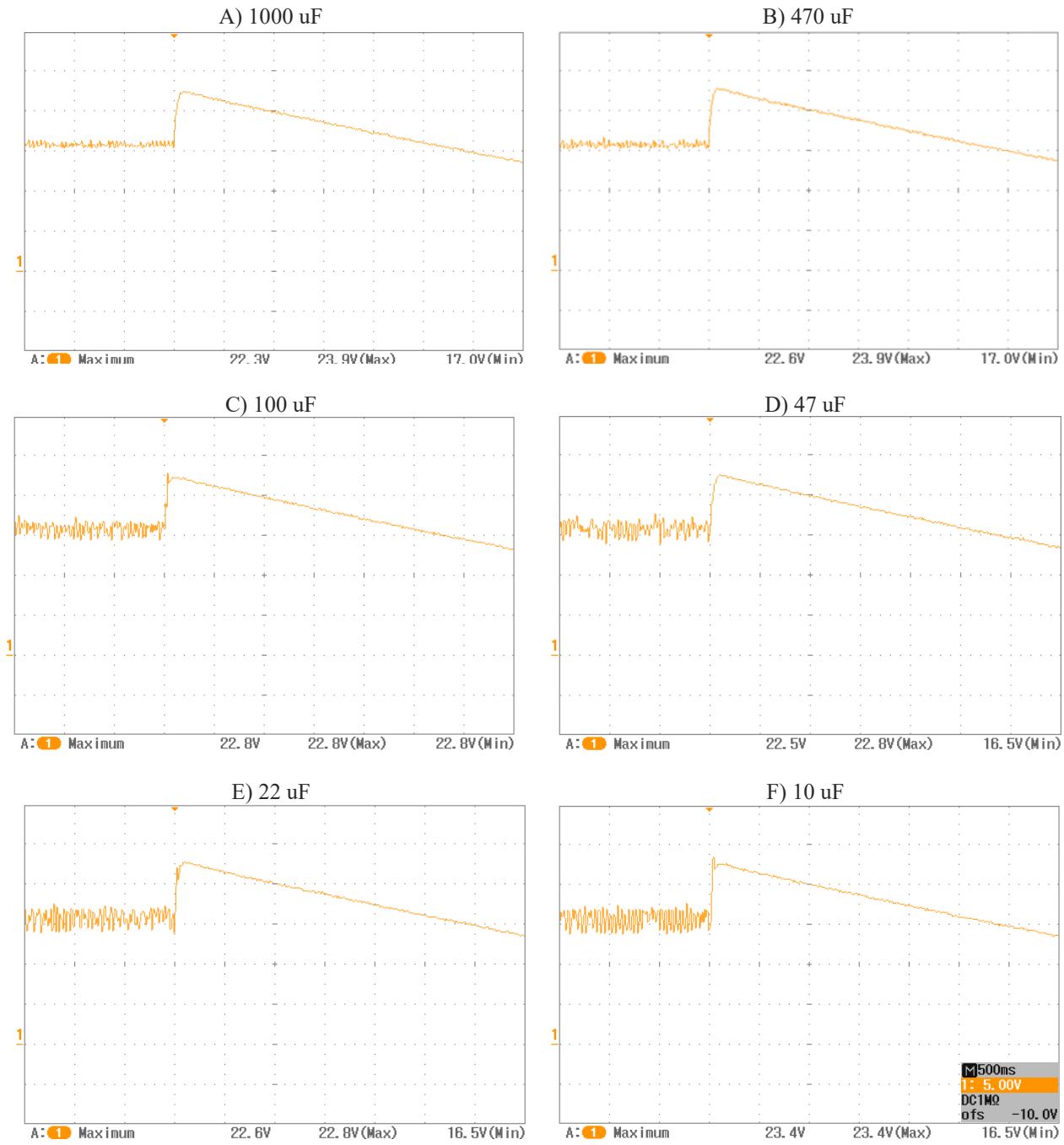

Figure 4.10: Smaller valued capacitors at 80 % thrust on 16.5 V / single 1700 Kv.
X-axis: Time [500 ms/div]. Y-axis: Voltage [5 V/div].

Although they help, the smaller capacitors do not reduce noise as much as the bigger 470 and 1000 uF capacitors do.

Finally, the 18 V TVS diode with the 470 uF capacitor was tested together in parallel, compared to baseline in Figure 4.11.

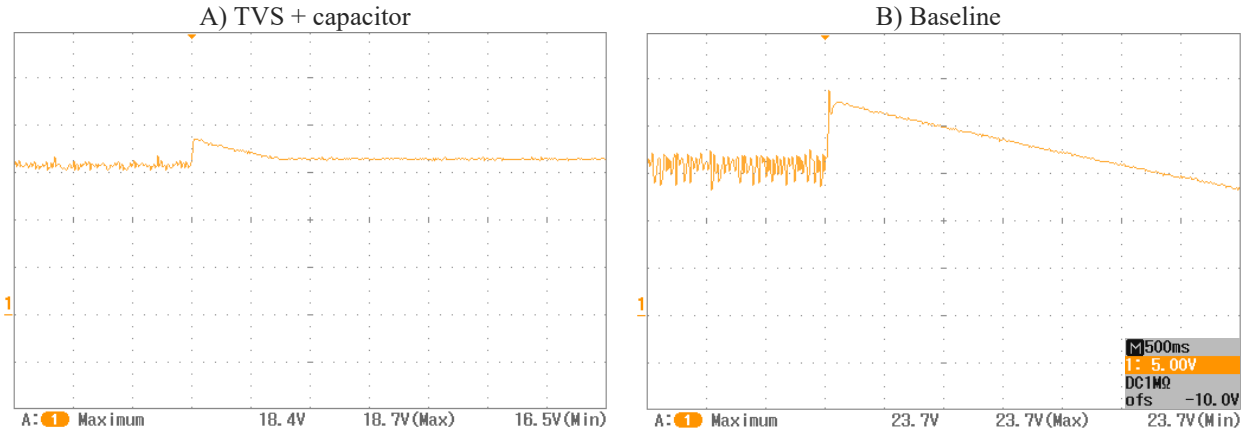

Figure 4.11: 18 V TVS + 470 uF capacitor in parallel at 80 % thrust on 16.5 V / single 1700 Kv. X-axis: Time [500 ms/div]. Y-axis: Voltage [5 V/div].

This combination of diode and capacitor gives the best results, where the diode clamps the voltage and prevents the PSU from shutting down, while the capacitor reduces the noise and ripples.

4.3 Low voltage response part 2 (15.0 V)

Some equipment in the drones from Scout had maximum ratings of 18 V, so it was of interest to see if the transient could be kept under this, alleviating the need for an additional buck converter before the payload. Since the diodes from the previous section did not fulfill this requirement, a 16 V TVS diode was tested (see Table 4.3 for specifications). Consequently, the supply voltage needed to be lowered.

This section shows transient response results from 15 V supply on 1700 Kv motors.

4.3.1 Single motor with components zoomed in

Up until now the plots have been shown with 500 ms/div. A 16 V TVS diode was tested and the current through it measured. The results at 100 % thrust and zoomed in are shown below.

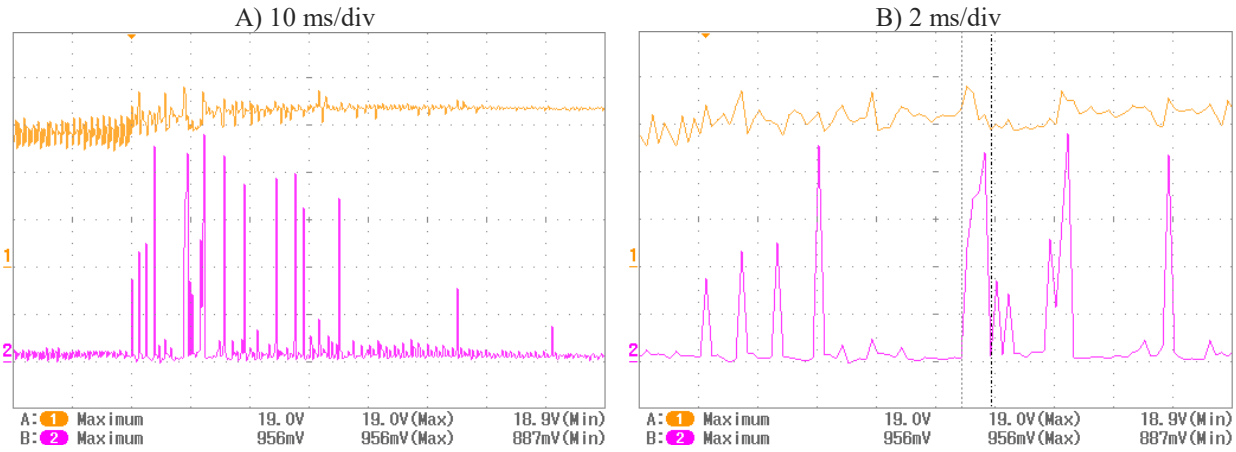

Figure 4.12: Response with a 16 V TVS at 100 % thrust on 15 V / single 1700 Kv.
X-axis: Time. Y-axis: Voltage in yellow [5 V/div], diode current in purple [6.2 A/div (200 mV/div)].

During steady state the mean current draw was 25.1 A. The voltage starts rising about 2 divisions from the left (the trigger is marked by the top arrow), and several impulses of current flow through the diode in a period of about 70 ms as seen in plot A. A closer, zoomed in look of these bursts is seen in plot B. One of the highest impulses is marked and measured about 900 mV/div which equals 27.5 A:

$$\left(900\ \frac{mV}{div}\right) \cdot \left(30.6\ \frac{A}{V}\right) = 27.5\ A$$

This corresponds well to the average current draw before the power cut. In general, these impulses were very short, the longest one being 1 ms.

However, the peak voltage measured was 19 V, which is too high, and well above the diode's breakdown rating at 16 V. The current sensor which was placed between the diode and ESC added some extra distance. The sensor was removed so that the diode could be placed directly onto the ESC. A 470 uF capacitor was also added for comparison. The result is shown in Figure 4.13.

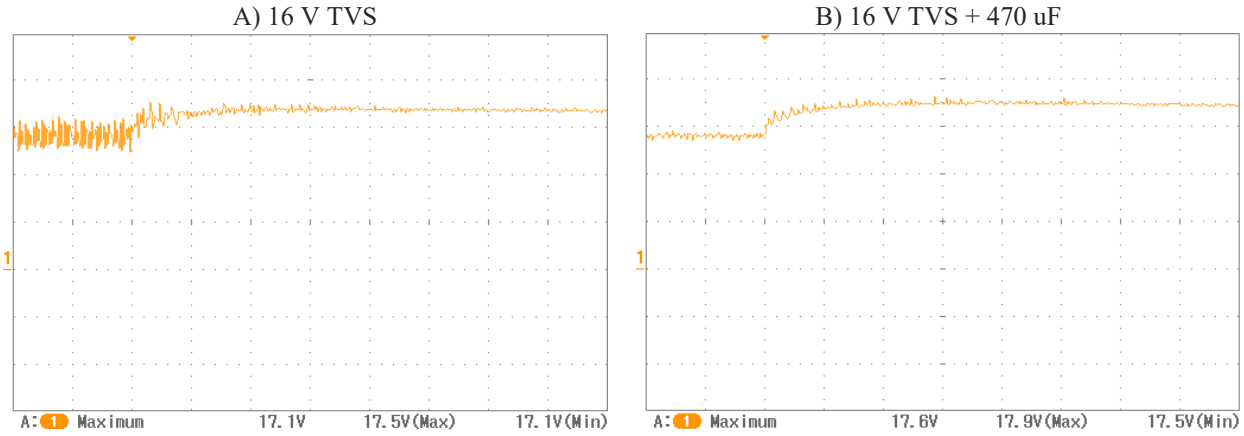

Figure 4.13: The components placed directly on the ESC at 100 % thrust on 15 V / single 1700 Kv.
X-axis: Time [10 ms/div]. Y-axis: Voltage [5 V/div].

Comparing the voltage in Figure 4.12-A and Figure 4.13-A it is seen that the transient ripple smaller, and the maximum measured voltage only 17.1 V (almost 2 volts less). Placement of the TVS diode is therefore significant, i.e. better when closer to the ESC (the source). The improvements from adding a capacitor in addition to the diode is evident as seen in plot B, especially on the ripple during steady state.

4.3.2 Quad motor testing on Woody

Quad motor response on Woody is summarized in Table 4.5. Figure 4.14 shows baseline response and Figure 4.15 shows added components.

Current draw is omitted, since the Betaflight [28] software used to control Woody could not show current nor could the PSU.

Table 4.5: Peak voltages in volts [V] for different components on 15 V / Woody.
The other entries than baseline are TVS diodes and a capacitor. “2x” means two in parallel etc.

Thrust	*Baseline*	*1x 16 V*	*2x 16 V*	*2x 16 V + 470 uF*	*3x 16 V*
20 %	18.7	n/a	n/a	n/a	n/a
40 %	24	n/a	n/a	n/a	n/a
60%	29.3	18.4	17.1	17.5	17.1
80 %	32.8	18.7	17.5	17.8	17.3
100 %	34.3	19	17.5	18.1	17.3

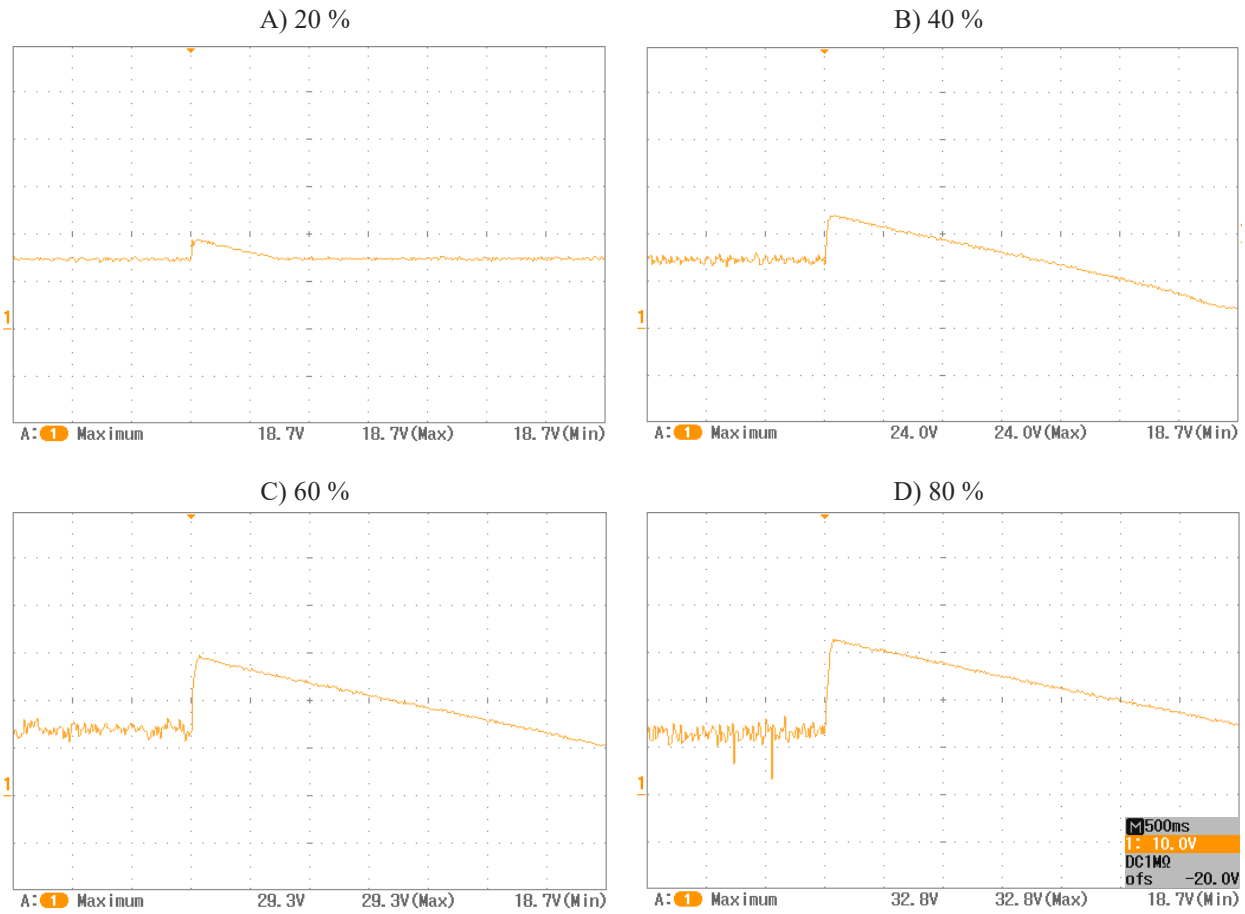

Figure 4.14: Baseline response on 15 V / Woody.
X-axis: Time [500 ms/div]. Y-axis: Voltage [10 V/div].

Figure 4.14 shows that the PSU shuts down at 40 % thrust from a peak of 24 V, since the voltage keeps dropping after the spike. At 80 % the voltage peaks at 32.8 V, over twice the nominal voltage.

A capacitor and up to three TVS diodes were added in parallel on the ESC, as shown in Figure 4.15.

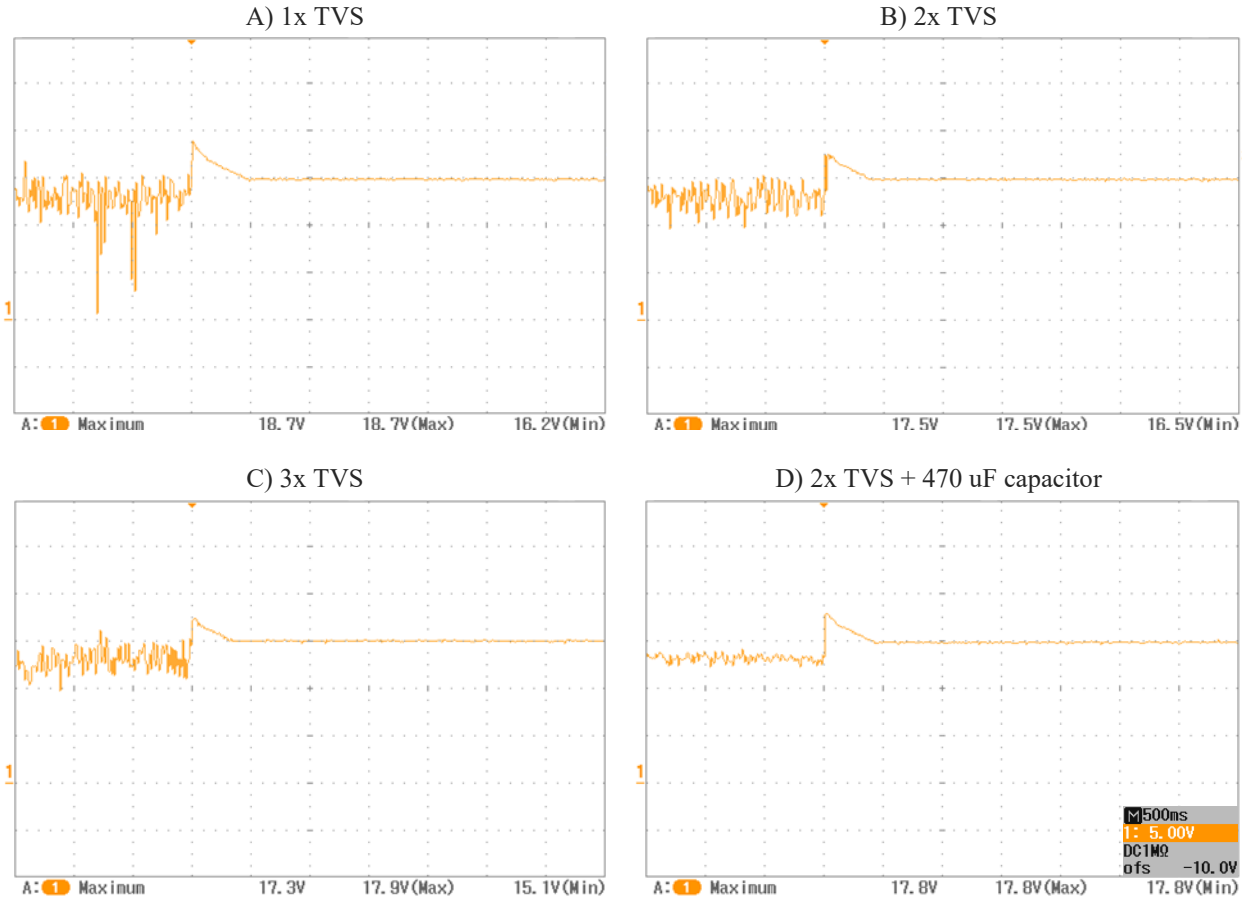

Figure 4.15: Combinations of 16 V TVS diodes and 470 uF in parallel at 80 % on 15 V / Woody. X-axis: Time [500 ms/div]. Y-axis: Voltage [5 V/div].

The PSU never shut down when protected by the diode(s). A single diode clamps the transient to 18.7 V at 80 % thrust, down from 32.8 V at baseline. However, it is not enough to keep the voltage below 18 V. Adding another identical diode in parallel to share the impulse current reduces the peak even further, down to 17.5 V at 80 %. Three diodes in parallel did not improve upon two significantly, showing no difference at 60 % and only a 0.2 V improvement at 80 %.

At 100 %, the peak voltage is reduced from 34.3 V at baseline to 18.1 V with two diodes and a capacitor (53 % reduction). Alternatively, the ΔV from 15 V to peak is reduced from a 128 % increase down to 20 %.

Adding a 470 uF capacitor to the two diodes raises the peak slightly but improves the steady state ripple notably, making this possibly the best combination.

Chapter 5
High voltage system power quality

This chapter shows results related to the power quality of the high voltage system, including transmission losses and transient response.

5.1 Transmission losses

The two cables on hand (Helukabel, see section 3.2.1) were tested for voltage and temperature at 50 meters. The two conductors were connected to a variable power supply and shorted on the other end. The voltage was then raised until approaching either 4 A or 40 V. Temperature was measured with a thermal imaging camera.

See Figure 5.1. The 0.14 mm^2 cable had a 38.73 V drop with 3.02 A passing through it, and a maximum measured temperature of 28 °C. The resistance is then found from Ohm's law:

$$R = \frac{38.73\ V}{3.02\ A} = 12.8\ \Omega$$

Dividing this by the length yields 256 mΩ per meter[c].

Since the APU needs a minimum of 260 V input voltage to function [16], a voltage drop above 40 V should be avoided. Thus the 0.14 mm^2 cable is unsuitable if left at 50 meters.

The 0.25 mm^2 cable had a 27.01 V drop with 3.99 A passing through it, and a measured temperature of 28.7 °C. The resistance was 6.77 Ω or 135 mΩ per meter, nearly half that of the 0.14 mm^2 cable. This cable could therefore be used at 50 meters.

The 0.14 mm^2 cable was cut to approximately 30 meters and measured once again at 24 V drop with 2.97 A passing through, as seen in Figure 5.2. This equals a resistance of 8.08 Ω, which

[c] Per meter of total cable length. Note that the even though the voltage is distributed over both the high and ground conductors, i.e. twice the cable length, this does not affect calculations. The effective voltage difference available on the ESC is still $V_{SUPPLY} - V_{TETHER}$.

is close to 3/5 of the previous value and expected since the internal resistance should be linear with the length of the cable.

A) Voltage drop on 0.14 mm^2

B) Thermal image on 0.14 mm^2

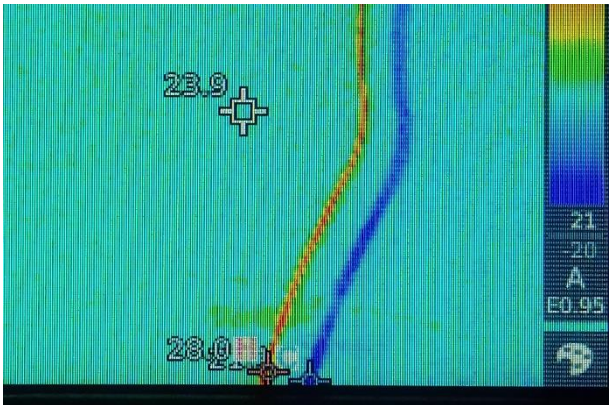

C) Voltage drop on 0.25 mm^2

D) Thermal image on 0.25 mm^2

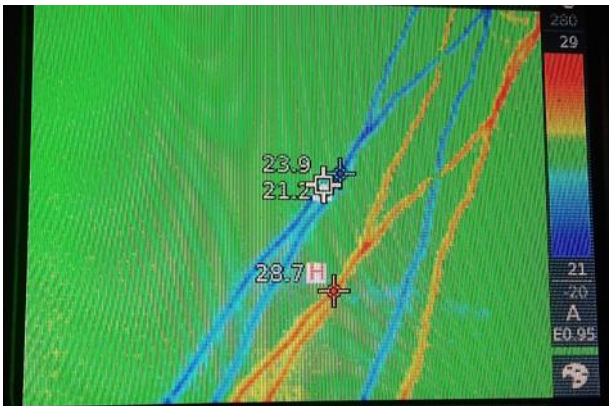

Figure 5.1: Voltage and temperature over 50 meter, 0.25 mm^2 and 0.14 mm^2 cables.

Figure 5.2: Voltage drop over 30 meter 0.14 mm^2 cable.

The voltage drop over the tether, V_{TETHER}, can then be calculated using Ohm's law. At 1500 W output from the PSU, i.e. 5 A the theoretical drop is slightly above 40 V:

$$(8.08\,\Omega) \cdot (5\,A) = 40.4\,V$$

Further, the power dissipation over the tether at 5 A would equal 202 W:

$$P_{TETHER} = (5\,A)^2 \cdot (8.08\,\Omega) = 202\,W$$

However, this power will be lost to the APU, which effectively only sees 1298 W. The required PSU output for a given APU output is found by the quadratic equation:

$$P_{PSU} = P_{TETHER} + P_{APU}$$
$$P_{PSU} = \left(\frac{P_{PSU}}{V_{PSU}}\right)^2 \cdot R_{TETHER} + P_{APU}$$

$$\frac{R_{TETHER}}{(V_{PSU})^2}\,P_{PSU}^2 - P_{PSU} + P_{APU} = 0 \tag{5.1}$$

For example, substituting V_{PSU} = 300 V and peak drone consumption P_{APU} = 1500 W,

$$\frac{8.08}{(300)^2}\,P_{PSU}^2 - P_{PSU} + 1500 = 0$$

the equation has solutions at P_{PSU} = 1786 and 9352 W, where the higher value can be discarded. This means the PSU must output at least 1786 W to deliver 1.5 kW to the APU[d]. Similarly, at hover (800 W) the PSU needs to output 868 W. At 400 V, the PSU output would need to be 1635 W and 835 W during peak and hover, respectively.

Note that, as mentioned in section 3.3.1, a 300 V supply cannot deliver 1500 W through the APU regardless due to output current restriction. A 400 V supply can, but the voltage drop must be less than 16 V (V_{PRI} = 384 V ⇒ V_{SEC} = 24 V):

$$P_{APU,SEC} = 24\,V \cdot 62.5\,A = 1.5\,kW$$

[d] This is disregarding the internal losses in the APU. The peak efficiency of the BCM chip at 1.5 kW is 97.2 % [16].

Figure 5.3 plots the input voltage V_{PRI} on the APU and transmission losses P_{TETHER} at variable power output on the PSU at 300 V.

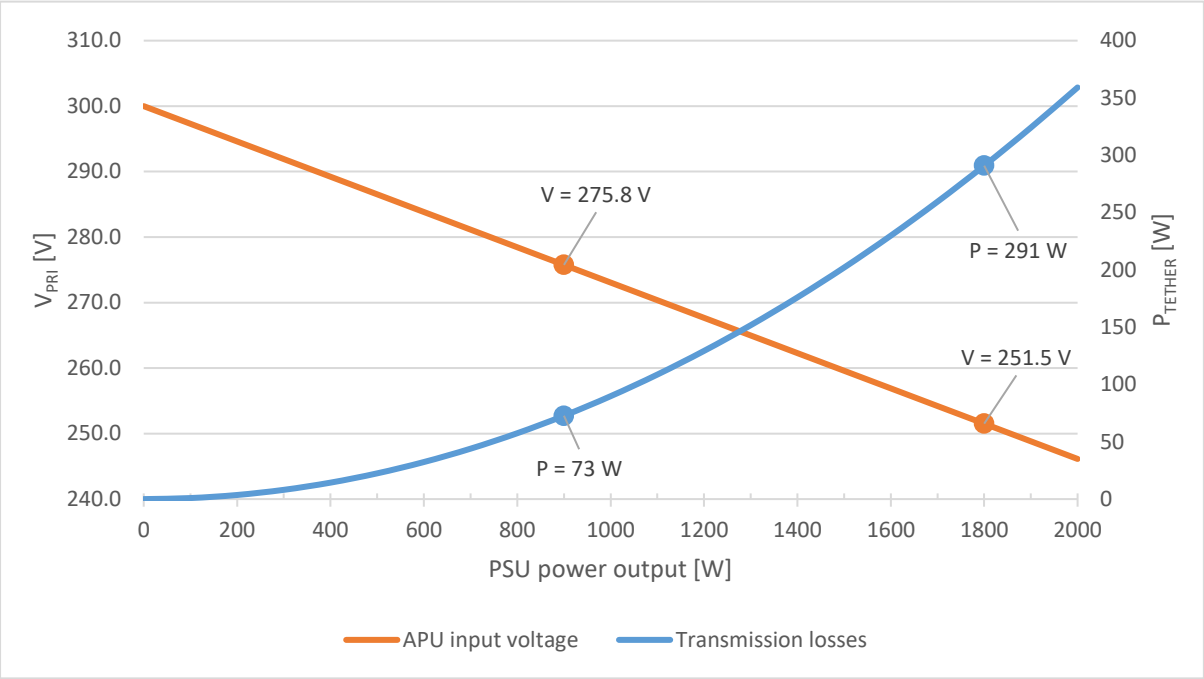

Figure 5.3: Input voltage and transmission losses as a function of PSU power output at 300 V. Input voltage in orange on left y-axis, power losses in blue on right axis.

The marked points are at 900 W and 1800 W output on the PSU, slightly above hover and peak drone consumption. In theory, peak consumption drops the voltage under 251.5 V, which is outside the operating range of the APU. In the span from hovering to peak consumption, the transmission losses are quadrupled from 73 W to 291 W.

Using equation 5.1 to adjust the PSU output for hover and peak at different voltages, the variation in input voltage and transmission losses can be calculated and plotted.

Figure 5.4 shows the input voltage on the APU. It is seen that 310 V on the PSU is sufficient to ensure that the input voltage is within the operational range of the APU.

Figure 5.5 shows transmission losses over the tether. Increasing the supply voltage further from 300 to 400 V can reduce the transmission losses by 33 W during hover, or by 152 W at peak (a 47 % decrease). Besides the fact that a 300 V PSU cannot deliver 1.5 kW through the APU anyways, this reduction in transmission losses is another strong advantage of a 400 V system. The recommended PSU from MEAN WELL [13] delivers up to 3 kW at 400 V which is more than enough to reach the peak target. Any other 400 V supply would suffice, but should be rated at 1700 W minimum to give some headroom.

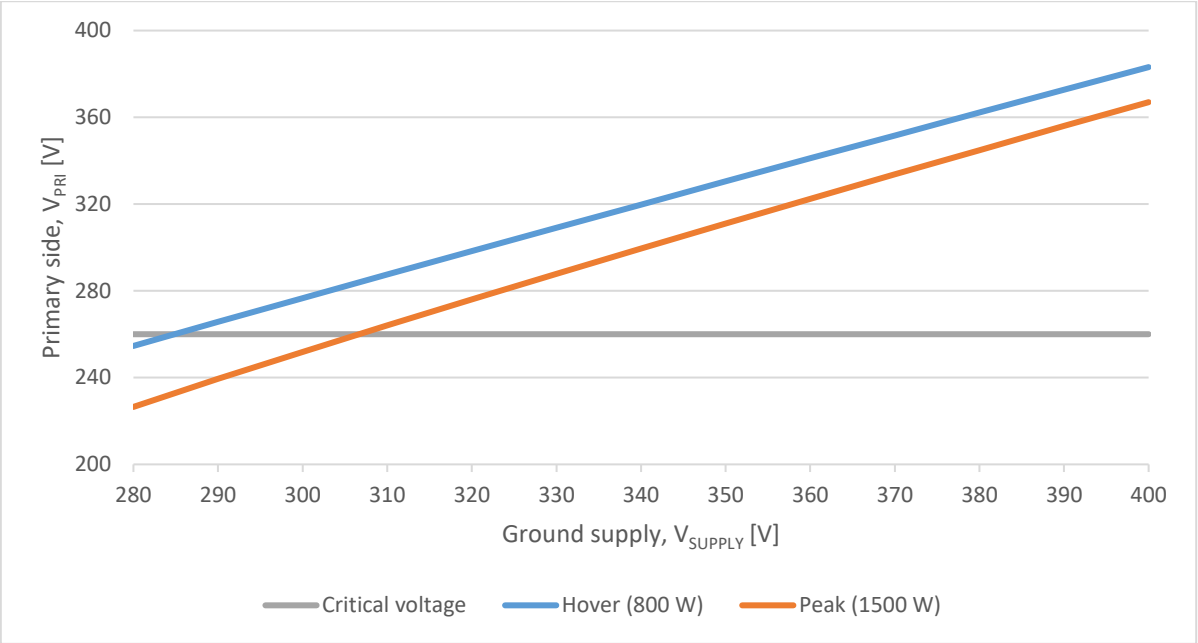

Figure 5.4: APU input as a function of supply voltage.

Blue and orange are P_{APU}, the critical voltage is 260 V.

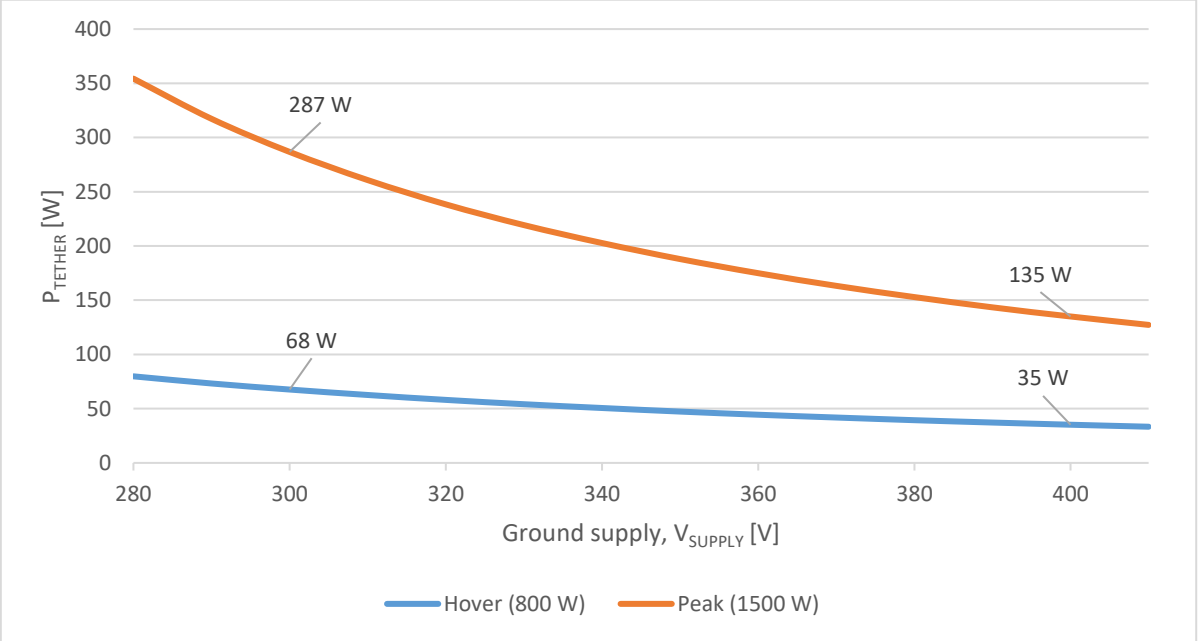

Figure 5.5: Transmission losses over the tether as a function of supply voltage.

Blue and orange are P_{APU}.

5.2 Transient response

This section shows transient response on the high voltage platform. The output voltage of the APU is expected to be 18.75 V nominal under no load after the conversion factor of 1/16.

5.2.1 Measuring transients

See section 4.1 for measuring procedures and how to read plots.

5.2.2 Baseline

The baseline measurements on the high voltage platform (300 V supply on Woody) are shown in Table 5.1 and the Figure 5.6.

Note that the current measured is from the high voltage PSU, and thus much lower than values from the LV platform. The temperature is the internal case value given by the TM pin on the APU and shown in purple on probe 2 in the plots. It is given by a reference 1.27 V = 27 °C and a gain of 10 mV/°C [16].

The voltage is measured on the secondary side of the APU, on the ESC as before on the low voltage platform.

Table 5.1: Baseline values measured on high voltage platform.
Current from PSU. Peak voltage on the low voltage side (ESC). Temperature from the APU.

Thrust	*Current [A]*	*Power [W]*	*Peak voltage [V]*	*Temperature [°C]*
20 %	0.26	78	19.6	54
40 %	1.08	324	20.7	55
60 %	2.48	744	23.1	46
80 %	4.3	1290	22.6	54

The temperature is not meant to simulate a real use case, since the APU was located very close to the propellers and thus received active cooling from the airflow. This is suggested by the lower temperature observed at 60 % thrust when the airflow is greater. At 80 % the power consumption in the APU is high which likely mitigates the increased airflow. Regardless, the maximum operational temperature of 125 °C [16] is unlikely to be reached during testing.

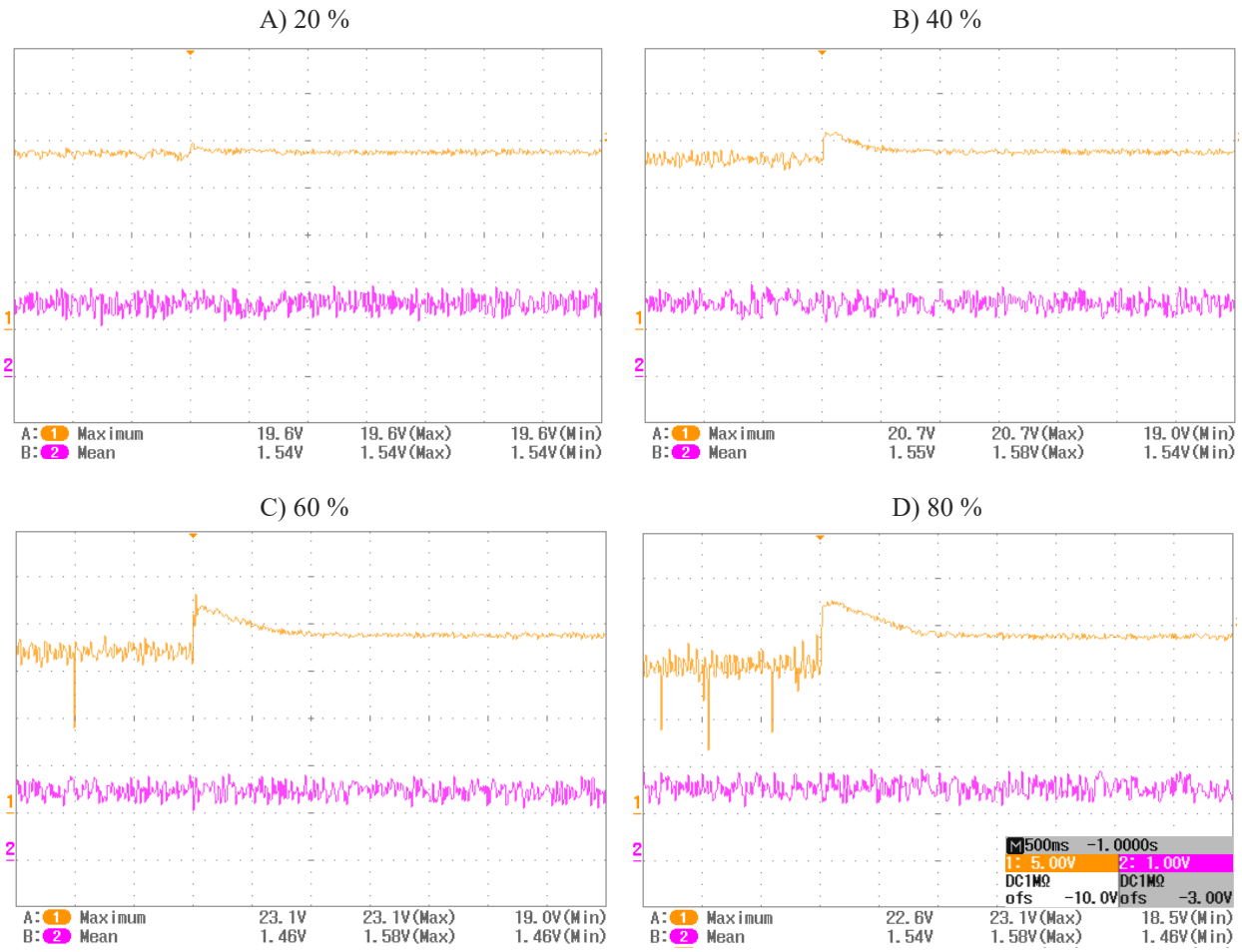

Figure 5.6: Baseline response on high voltage plat form.

X-axis: Time [500 ms/div]. Y-axis: Voltage in yellow [5 V/div], temperature in purple (see text above).

The highest increase observed is 23.1 V, a 23.2 % rise from the nominal voltage. The voltage transients are also much better by default than the simulated, LV platform. The peak at 80 % is only 22.6 V, compared to 32.8 V as was seen in Figure 4.14. The entire system also does not shut down in the transient as previously observed on the LV platform, as the voltage simply returns to the nominal level. In this regard the high voltage platform is inherently much more robust even without protective components.

5.2.3 With protective components

A 450 V, 10 uF capacitor was installed on the primary side (high voltage), following the reference design from Vicor [18]. In addition, 20 V TVS diodes and a 470 uF capacitor (35 V) were added on the secondary side, on ESC similar to the tests on the low voltage system. The results are shown in Table 5.2, Figure 5.7 and Figure 5.8.

Table 5.2: Peak voltages in volts [V] for different configurations on the high voltage system. "Reference" is a 450 V / 10 uF capacitor on the primary side. The other entries are TVS diodes and a capacitor on the ESC *in addition* to the primary side capacitor. "2x" means two in parallel.

Thrust	*Reference*	*1x 20 V*	*2x 20 V*	*470 uF*	*1x 20 V + 470 uF*
40 %	20.6	20.6	20.6	20.9	20.6
60 %	22.3	21.2	21.2	21.8	21.4
80 %	n/a	n/a	n/a	22.6	21.7

Comparing baseline response in Figure 5.6 to the response with the reference, high voltage capacitor in Figure 5.7, there does not seem to be much improvement. At 60 %, the spike is 23.1 V at baseline compared to 22.3 V on the reference capacitor, but it is seen that there is a ripple during the transient in Figure 5.6-C which could be at random (recall that the baseline peak was 22.6 V at 80 %, less than at 60 %).

A 20 V TVS diode reduces the peak to 21.2 V compared to the reference 22.3 V. Adding two diodes in parallel does not reduce the peak further, unlike results observed on the low voltage platform in section 4.3.2 where two diodes was beneficial.

A 470 uF capacitor alone reduces the peak down to 21.8 V, better than reference but not than the TVS diode. It improves the ripples significantly as seen in Figure 5.8-C.

A diode and capacitor in parallel reduce the peak to 21.4 V. This is better than just a capacitor, but still slightly worse than just a diode, similar to the observation on the low voltage platform. The combination of diode and capacitor still may be the best option, however, due to the improvements on steady state ripples. The voltage rise from the nominal 18.75 V is only 14.1 %, down from 23.2 % in the baseline.

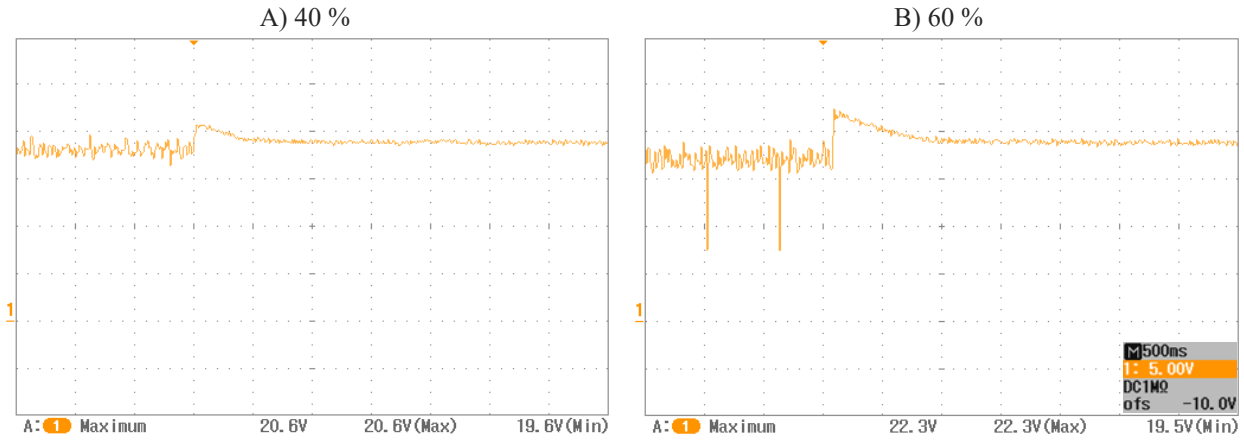

Figure 5.7: Response with a 450 V 10 uF capacitor (reference design) on the primary side.

X-axis: Time [500 ms/div]. Y-axis: Voltage [5 V/div].

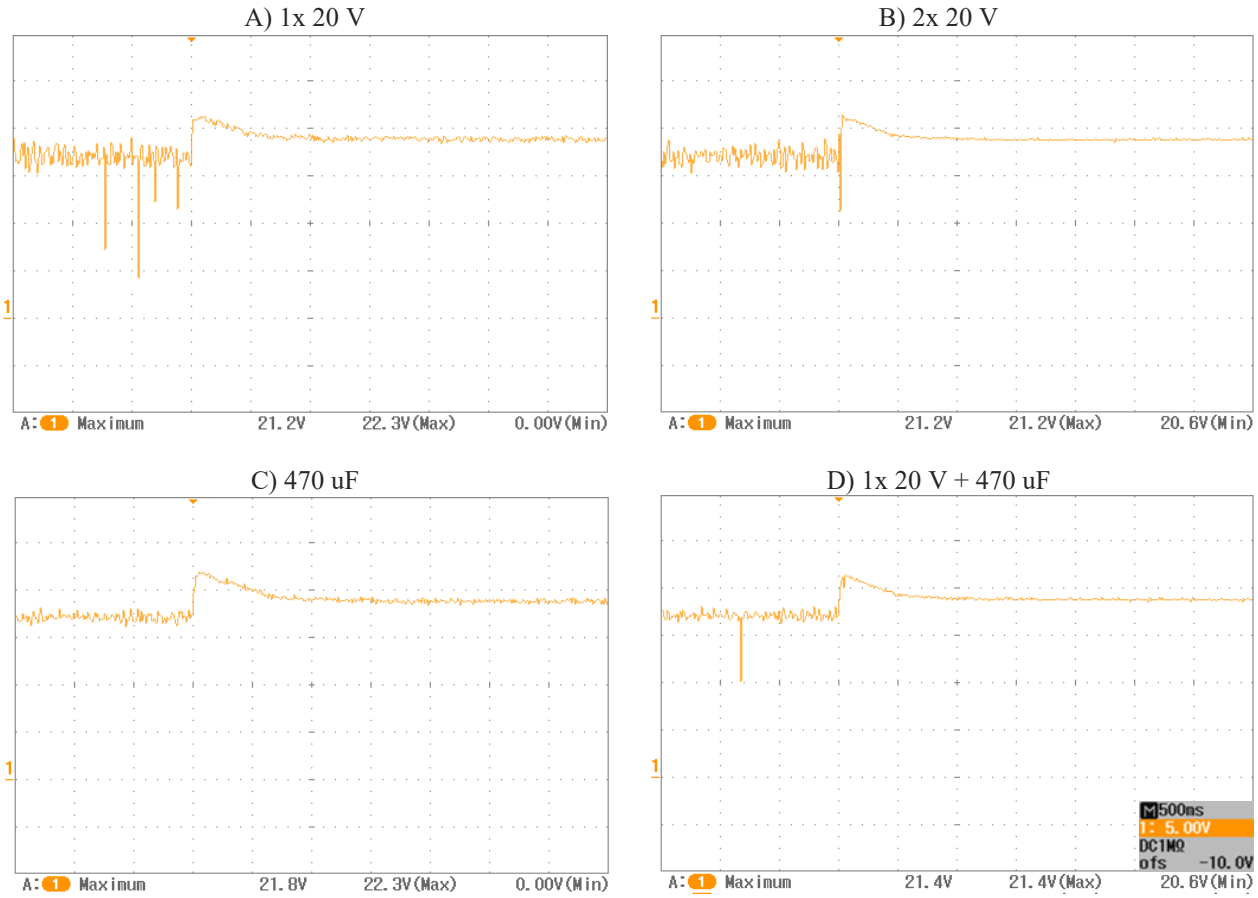

Figure 5.8: Different configurations of TVS diodes and a capacitor on the ESC at 60 % thrust.

X-axis: Time [500 ms/div]. Y-axis: Voltage [5 V/div].

5.2.4 With filters

The APU PCB was designed with optional ways to add extra filters, see section 3.3.2. The transient voltages on the ESC at 60 % thrust are shown in Figure 5.9.

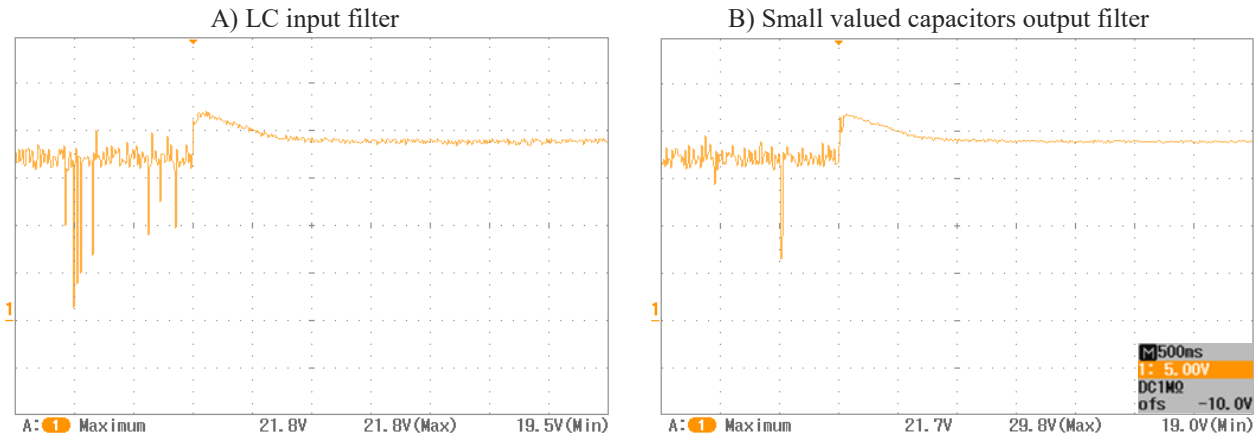

Figure 5.9: Response with an input and output filter at 60 % thrust.
X-axis: Time [500 ms/div]. Y-axis: Voltage [5 V/div].

Compared to the reference in Figure 5.7-B, both filters reduce the voltage peak by up to half a volt. The steady state ripple is slightly improved with the output filter, while the input filter seems to worsen the ripple. No significant useful effect is observed with the filters compared to the results with protective components directly on the ESC.

5.3 Step response and inrush current

There was a consistent problem where the APU would reboot when the thrust was stepped from low to high very fast, i.e. from 0 to 70 % thrust (since 80 % and above was unstable due to power limits). The reboot happened in all configurations and made the ESC unable to start the motors. Figure 5.10 shows the reboot in the baseline configuration.

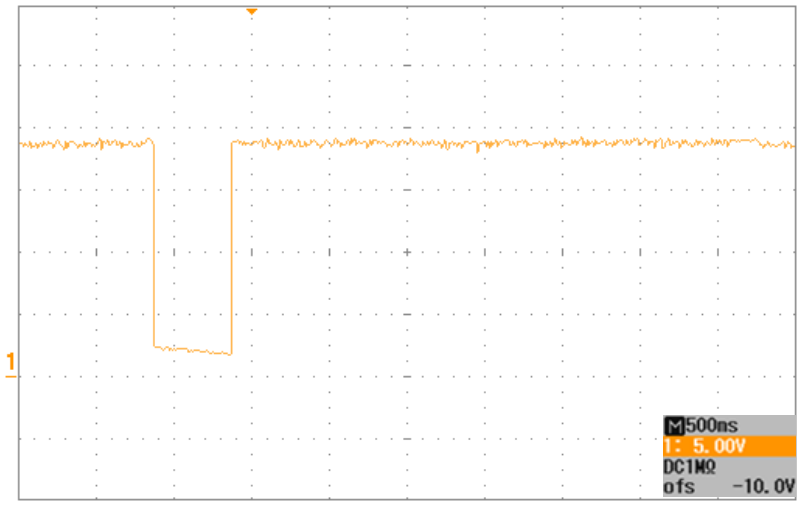

Figure 5.10: APU rebooting after stepping the motor from low to high rpm.
X-axis: Time [500 ms/div]. Y-axis: Voltage [5 V/div].

The large dip in voltage is the BCM chip on the APU shutting down. The auto-restart time of the chip is from 490 to 560 ms [16] which matches the observed dip well. There are only a few events that could trigger a shutdown:

- Primary/secondary overvoltage
- Primary/secondary undervoltage
- Primary/secondary overcurrent
- Overtemperature
- Undertemperature

It was suspected that the large inrush current during motor startup was the cause. The datasheet lists a secondary overcurrent threshold of min 75 A, typical 84 A and max 110 A. Probing the current during a test revealed an inrush peaking at 103 A before the APU shut down, as seen by the voltage collapse in Figure 5.11. Note that since the APU shut down, the maximum current that could have occurred remains unknown.

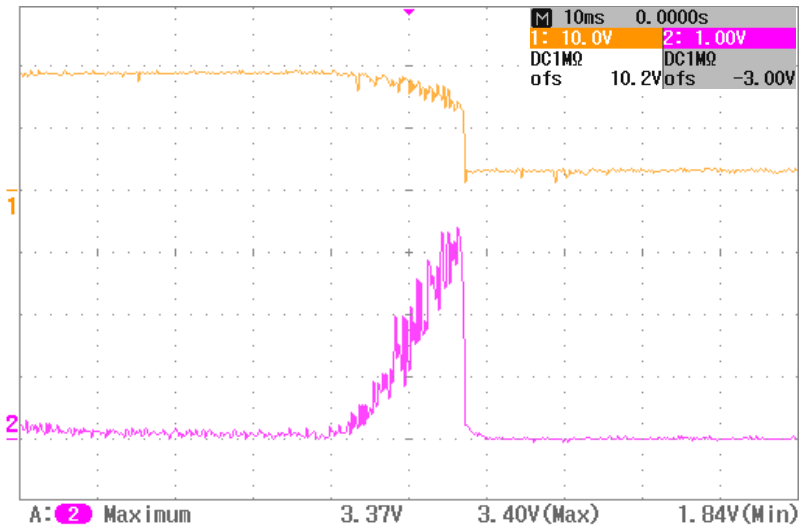

Figure 5.11: The inrush current when stepped from low to high rpm.

X-axis: Time [10 ms/div]. Y-axis: Voltage in yellow [10 V/div], current in purple [30.6 A/div].

The solution to dealing with large inrush currents in motors is to gradually increase the speed or limit the ramp-up power. The flight controller had two relevant parameters: “Rampup power” and “Maximum acceleration”. Explaining how they work and tuning Woody optimally is beyond the aim of this report, however after some runs it was discovered that limiting the Maximum acceleration parameter to 0.8 %/ms was stable, as seen in Figure 5.12. Values up to 1.2 were also stable, despite yielding peak currents of 104 A, but 0.8 would be a safer choice and did not impact the responsiveness of the drone either.

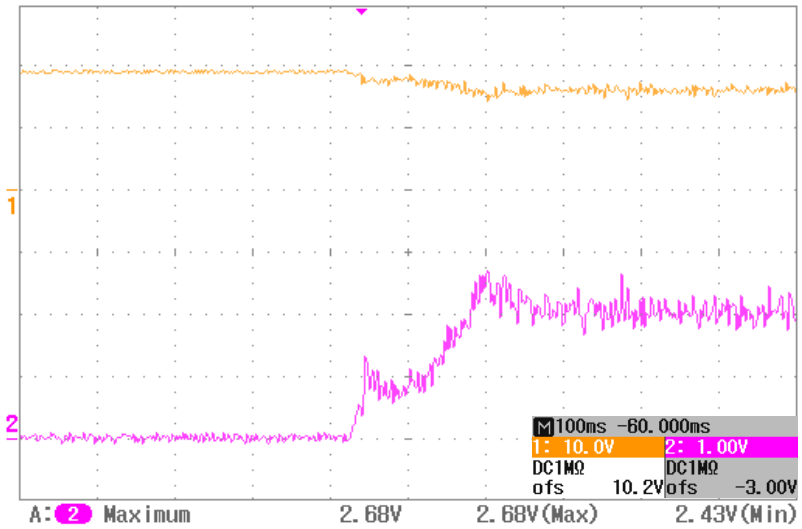

Figure 5.12: Ramp-up and inrush current with Max. acc parameter set to 0.8 % / ms.

X-axis: Time [100 ms/div]. Y-axis: Voltage in yellow [10 V/div], current in purple [30.6 A/div].

Another solution than tuning would be to use the battery interface to take over during instances of large inrush current. This is seen in Figure 5.13, where the voltage starts to drop, then the battery picks up during the APU down-time, and finally the APU turning on and powering the motors (now at a lower voltage due to load). Note that purple in this figure is not current, but the ON/OFF signal from the APU from the V_{AUX} pin.

It is however advisable not to rely on the battery as a replacement for ramp-up limitation due to unreliability (see section 6.3.2 where the APU doesn't switch back), and since inrush current should generally be avoided.

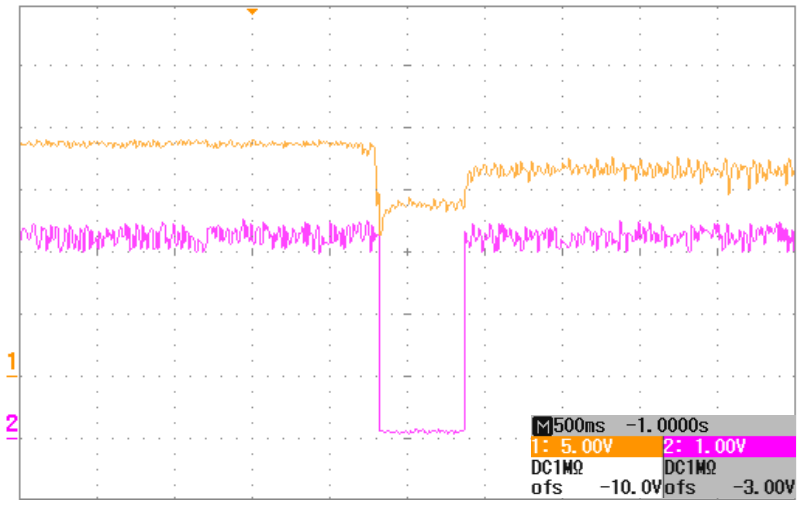

Figure 5.13: Stepping from low to high rpm with the active battery interface installed.
X-axis: Time [500 ms/div]. Y-axis: Voltage in yellow [5 V/div], V_{AUX} pin in purple (High:ON / Low:OFF).

Chapter 6

Final system tests and results

This chapter presents the final results, using the solutions found to be best from the previous chapters.

6.1 Final system cost estimate

A rough cost estimate was made for the entire system based on the prices where the components were bought:

Table 6.1: Cost estimate of the entire system, based on retail prices and excluding shipping.

	Total price [USD]	*Supplier*	*Parts included*
Vicor BCM chip	207	digikey.com	1x [16]
Battery interface	6.8	tme.eu	2x [22] + 2x [23]
Data link	77	aliexpress.com	2x [25]
Tether	23	tme.eu	30 m [10]
Power supply	326	ebay.com	1x [11]
PCB	5	jlcpcb.com	1x

Thus, a total of $648 could be expected for this system, excluding shipping.

If the system is upgraded with the MEAN WELL CSP-3000-400 power supply [13], which costs $447, the total price would be $769.

6.2 Air power unit and flight

As a final result on the high voltage platform, Woody was equipped with:

- 10 uF, 450 V input capacitor on the APU,
- 470 uF, 35 V and 20 V TVS diode on the ESC and
- the flight controlled tuned for inrush current.

The first test flight video can be seen by scanning the QR code in Video 1.

Video 1: First high voltage test flight on Woody.
URL: https://youtu.be/amP0d_XNogQ

The system performed above all expectations without any issues. The flight dynamics when dragging a tether is also demonstrated, where the tether is holding back the drone due to tension and weight.

6.3 Battery backup interface

6.3.1 Passive circuit

The passive circuit was installed on the low voltage platform on Woody with a backup battery connected. The current through the battery was monitored while turning the PSU on and off. The result is demonstrated in Video 2 (loud noise warning).

Video 2: Passive battery circuit test on low voltage platform on Woody (with captions).
URL: https://youtu.be/XUrYi6BChac

The circuit worked as expected, with basically zero current flowing through the battery while the PSU was on. When the PSU is switched off the response from the battery is immediate resulting in no downtime, and likewise when the PSU is turned on, the battery stops powering. The difference of voltage between switching is noticed by the change of rpm on the motors. The heatsinks and components felt cold to the touch even after several minutes of stress testing.

6.3.2 Active circuit

The active circuit was tested on the high voltage platform on Woody, see Figure 6.1.

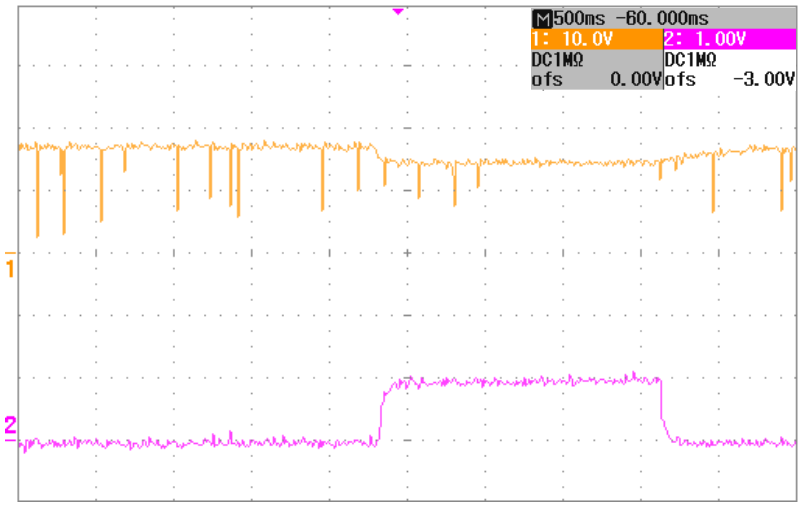

Figure 6.1: Active battery circuit test on high voltage platform.
X-axis: Time [500 ms/div]. Y-axis: Voltage in yellow [10 V/div], current in purple [30.6 V/div).

The current is zero while the PSU is on and goes up when the PSU is turned off simultaneously with a voltage drop to about 15 V (battery level). The circuit works as expected.

The circuit was also tested on one of Scout's prototype drones. A prototype air module was made on a wooden board with all the modules, as seen in Figure 6.2.

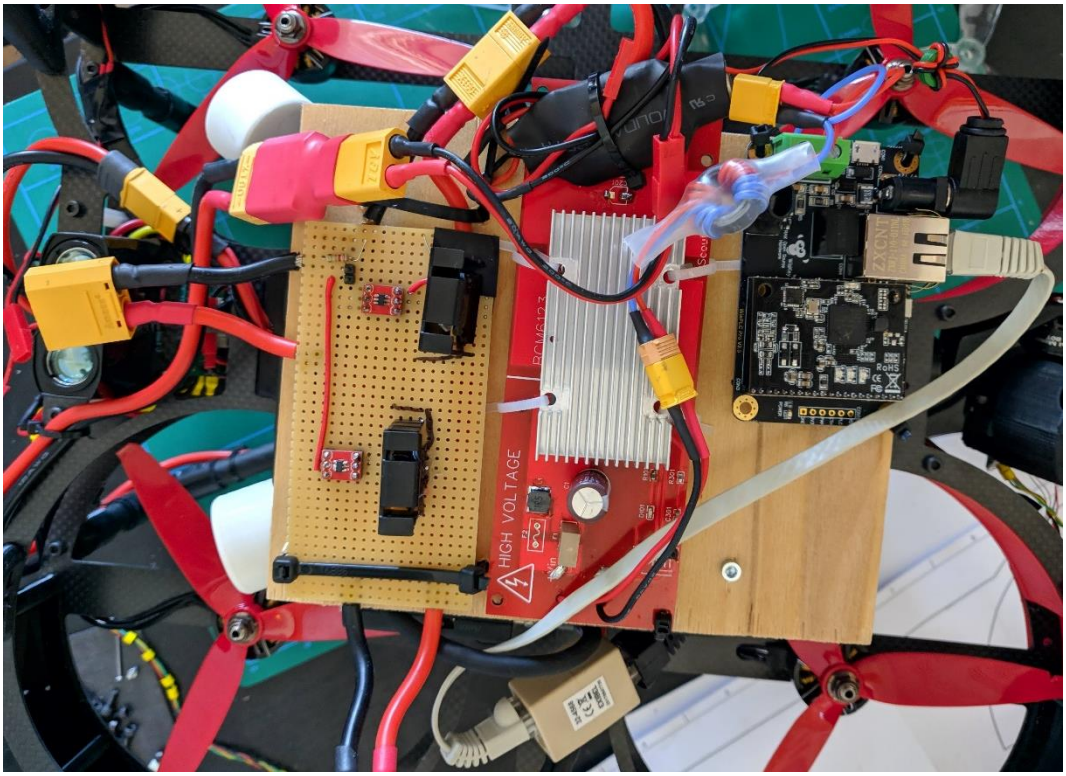

Figure 6.2: The backup battery interface, APU and data module installed on a real Scout drone.

The test flight is shown in Video 3 (loud noise warning).

Video 3: Active battery circuit test on a Scout prototype drone (with captions).
URL: https://youtu.be/7iy9bXUnvo0

The circuit was able to switch over to the battery as expected without interrupting flight much, except for a small fall in altitude due to the battery's lower voltage. However, as seen on the PSU, the output current remains zero when it is turned on again and the APU cannot switch back to power the drone. It is speculated that this is a limitation within the Vicor chip when the load is already significant. Controlled testing on Woody confirmed that there is a threshold where the APU can switch back, and where it cannot, around 600 to 800 W.

Although there was no time to test this, one possible solution could be to use the jumper P1 on the switchover circuit to trigger the OFF pin of the controller. This would force the battery's MOSFET off when the APU boots and possibly let it switch over.

Another observation worth noting is that this drone drew about 1160 W continuously, more than the target 800 W hover. It is thus too heavy or inefficient.

As commented in the video, the data link is lost when the PSU is switched off since it was powered from the APU output, and not the switchover circuit's output.

6.4 Data link

The data link was tested on one of Scout's drones that could livestream video from its camera. The livestream was lost when the modules were installed directly onto the power line without extra equipment. A bandwidth measurement tool, iPerf3 [29] was used to benchmark the network by connecting a computer to the RJ-45 port on the drone side and another computer to the port on the PSU side and running the tool. It was discovered that the bandwidth dropped when there was voltage on the tether (but no load), and dropping almost completely out when a current of 2.7 A was drawn, which equals 800 W at 300 V.

It was suspected that noise from the PSU and APU caused the bandwidth to drop, so differential mode chokes were made and installed (see section 3.5). Tests were done with no chokes, a choke by the PSU and two chokes on both ends. The UDP protocol was used with a target 100 Mbit/s, and run for 60 seconds each time, taking the average as result. The detailed results are shown in Table 6.2 at 800 W, see appendix A for the rest. Bandwidth comparison is shown in Figure 6.3.

Table 6.2: iPerf3 bandwidth results over 60 seconds on data link at 800 W (2.7 A).

	Bandwidth [Mbit/s]	*Jitter [ms]*	*Lost/Total Datagrams*
No chokes	2.96	146.9	501/2714 (18 %)
PSU choke	56.2	1.179	0/51430 (0 %)
Two chokes	93.1	0.492	0/85257 (0 %)

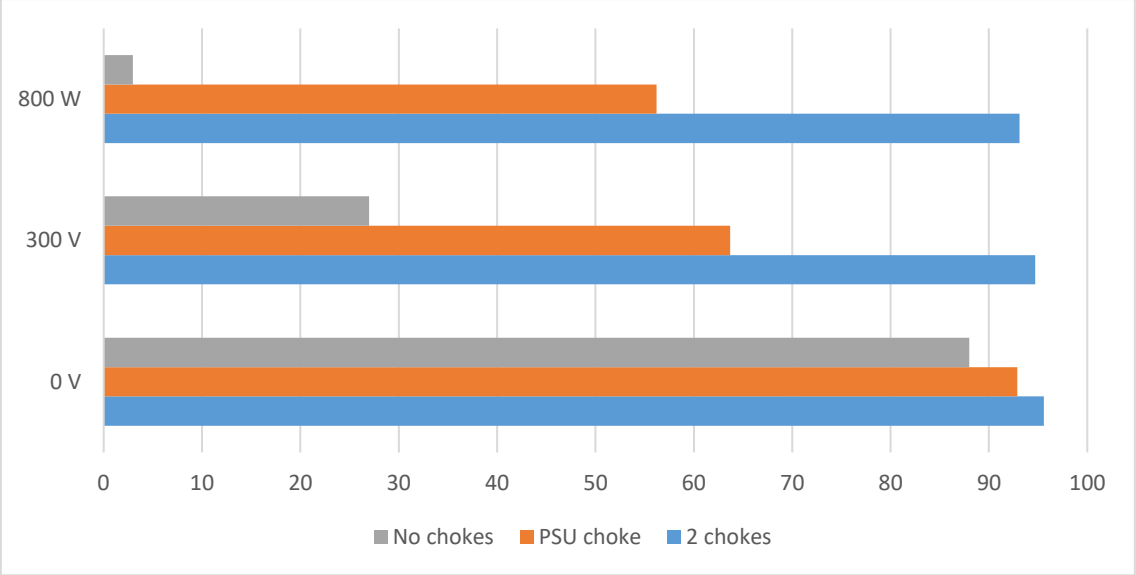

Figure 6.3: iPerf3 bandwidth results on data link. 0 V is with the PSU turned off. 300 V is with the PSU turned on, but no current drawn. 800 W is with the PSU on drawing 2.7 A.

With no chokes installed, the bandwidth dropped to 2.97 Mbit/s and with 18 % lost datagrams, explaining why the video stream was lost during tests. It is seen that the two chokes almost eliminate all the noise and keeps the bandwidth stable regardless of the load. A single choke on the PSU helps a great deal and could probably be sufficient, but it is recommended to use two chokes at both ends. It could be considered to use a better and heavier industrial choke on the PSU side and keeping a light-weight choke on the drone side.

Finally, the data link was tested on the Scout drone, see Video 4 (loud noise warning). The link was stable and didn't drop out, only very occasionally during take-off and landing. It is speculated that this is likely caused by an instable power delivery to the data module. Capacitors or better filtering on their supply input could solve it.

Video 4: Video stream over the data link demonstration on a Scout prototype drone.
URL: https://youtu.be/OYhHE0LYT0g

Chapter 7
Conclusions and further work

This report has presented a system for delivering power to a drone through a high voltage tether with a converter module onboard. The entire system, including a safety battery switchover system and a data link over the power line is estimated to cost about $648.

Voltage transients were discovered during rapid changes in motor throttle that affected the power quality and safety of the drone. Measures have been taken to prevent instability and improve the reliability of the power transmission and data connection. A summary is given in this chapter.

7.1 Power quality and delivery system

- A TVS diode can clamp the voltage transients at a safe level. Capacitors alone cannot keep the voltage at a safe level, but are useful for reducing the voltage ripples and noise on the bus. The best clamping and noise reduction are achieved by placing the components as close as possible to the ESC.
- For the low voltage platform which simulates the HV system, it is recommended to use two 16 V TVS diodes and a 470 uF capacitor in parallel on the ESC. This will reduce the peak voltage by up to 53 %.
- The real high voltage system is inherently much better at limiting voltage transients than the simulation. It does not shut down from disarming the motors, hence it does not need protective equipment for basic operation. In any case, it is recommended to use a single 20 V TVS diode and a 470 uF capacitor in parallel on the ESC. This limits the peak and reduces voltage ripples. A diode rated above 25 V should be used if the tether operating voltage is increased to 400 V. A buck converter is almost certainly necessary before the payload in the high voltage system.

- 300 V might be too low to maintain a stable APU input during heavy load due to voltage drop. It also cannot deliver the target 1500 W at the APU, falling just short of 1200 W. Additionally, the transmission losses can be reduced by up to 47 % at 400 V. It is therefore recommended to upgrade the tether and PSU to 400 V, [13] is a good choice.
- Inrush current can trigger a fault condition in the APU when increasing the motor rpm very fast. This will result in complete motor stop and should be avoided by limiting the ramp-up power or acceleration in the flight controller tuning software.

7.2 Air power unit

- The BCM fixed-ratio converter chip from Vicor [16] is a relatively cheap solution compared to the alternatives (mainly the regulated DCM chips). It can deliver the necessary 1500 W in a light and small package.
- The reference design from the datasheet a good, working foundation, but it is speculated that the input capacitor is unnecessary from test results.

7.3 Battery backup interface

- The active switching circuit works like expected in switching to the backup battery in case of mains supply failure. It is recommended to integrate the circuit as part of the APU, even if a battery isn't installed since it inherently provides reverse polarity protection which should be added to the system anyways. The current MOSFETs installed are very efficient and would only dissipate 3.5 W at peak power consumption.
- At the moment the APU cannot switch back to powering the drone if the switchover is already triggered and the battery is powering the device, likely due to a limit within the BCM chip. It is therefore necessary to land the drone safely as soon as possible in the case of mains supply failure. A possible solution could be to utilize the OFF pin on the gate controller for the battery path.

7.4 Data link

- A stable connection of at least 90 Mbit/s is achievable with the LX200V20 modules provided that differential mode chokes are installed between the tether and end terminals (PSU and APU).
- Without the chokes, the bandwidth basically drops out under significant load due to noise on the line. A simple, self-wound choke is sufficient, but it is recommended to integrate a professional choke as part of the input of a revised APU and in the eventual ground box housing the PSU and tether.

7.5 Further work

There are still some aspects worth investigating further in order to give better recommendations on a tethered system, and room for improvement and optimization on the solutions implemented.

It could be following:

- Investigating the cause of the voltage transients, which currently remain unknown. It is speculated that it is rooted in either back EMF from the motors or voltage sag and swell occurring when a load is suddenly added or dropped in the system. Finding the cause may give greater insight into the solution.
- Using a different oscilloscope to get raw data, on which transient energy can be calculated from voltage and current. Using the current and rise time to find a capacitor bank that could better absorb the energy.
- Integrating the battery backup interface (active circuit) as part of the output on a revised APU board. Also adding reverse polarity protection on the input of the APU, either by a ground side n-channel MOSFET or a series diode (the current and thus losses are low on the high voltage side).
- Developing a methodology for tuning the flight controllers to limit inrush current but preserve optimal performance and responsiveness.
- Developing a custom PCB for the LX200V20 data link and integrating this with the APU in a new housing (air module). This module should be stored in a ground box, where the tether, PSU and ground side data link are also housed for safe transport and easy deployment of the system.

References

[1] Goldman Sachs, “Drones: Reporting for Work.” [Online]. Available: https://www.goldmansachs.com/insights/technology-driving-innovation/drones/. [Accessed: 01-Mar-2019].

[2] Elistair.com, “Tethered system manufacturer (France).” [Online]. Available: https://elistair.com/. [Accessed: 28-Feb-2019].

[3] Bluevigil.com, “Tethered system manufacturer (USA).” [Online]. Available: http://bluevigil.com/. [Accessed: 28-Feb-2019].

[4] UNMND.com, “Drone and tether system manufacturer (UK).” [Online]. Available: http://www.unmnd.com/drone-tether-systems.html. [Accessed: 03-Apr-2019].

[5] A. Zawadzki, R. L. Adamski, and M. Slusarczyk, “Tethered aerial drone system,” 2016.

[6] B. Hartwig, “What is a Silicon Transient Voltage Suppressor and how does it work?,” 2007.

[7] A. Sedra and K. Smith, *Microelectronic Circuits, International Sixth Edition*. 2011.

[8] MEAN WELL, “PSPA-1000-15 Power Supply.” [Online]. Available: https://www.meanwell.com/webapp/product/search.aspx?prod=PSPA-1000. [Accessed: 13-Jun-2019].

[9] RCbenchmark, “Series 1580 Thrust Stand and Dynamometer.” [Online]. Available: https://www.rcbenchmark.com/pages/series-1580-thrust-stand-dynamometer. [Accessed: 13-Jun-2019].

[10] Helukabel, “SUPERTRONIC-PURO 49583.” [Online]. Available: http://www.helukabel.com/opc/workarea/suppliers/STD/documents/pdf/db/1DB_49583_en.pdf. [Accessed: 18-Jun-2019].

[11] ebay.com, “1500 W 300 VDC 5A PSU, factory direct sale.” [Online]. Available: https://www.ebay.com/usr/sheep20110812. [Accessed: 18-Jun-2019].

[12] igus, “chainflex CF98.01.02.” [Online]. Available: https://www.igus.com/contentData/Products/Downloads/CF98_sort131_Control_cable_USen.pdf. [Accessed: 03-Jul-2019].

[13] MEAN WELL, “CSP-3000 Series Power Supplies.” [Online]. Available: https://www.meanwell-web.com/en-gb/meanwell-csp-3000/. [Accessed: 03-Jul-2019].

[14] Vicor Corporation, “Isolated Fixed Ratio DC-DC Converters.” [Online]. Available: http://www.vicorpower.com/dc-dc/isolated-fixed-ratio. [Accessed: 09-Jul-2019].

[15] Vicor Corporation, “DCM4623TD2K17E0T00.” [Online]. Available: http://www.vicorpower.com/documents/datasheets/DCM4623xD2K17E0yzz_ds.pdf. [Accessed: 09-Jul-2019].

[16] Vicor Corporation, “BCM6123TD1E2663T00.” [Online]. Available: http://www.vicorpower.com/documents/datasheets/ds_BCM6123xD1E2663yzz.pdf. [Accessed: 03-Jul-2019].

[17] EasyEDA, “Online PCB design tool.” [Online]. Available: https://easyeda.com/. [Accessed: 10-Jul-2019].

[18] Vicor Corporation, “BCM6123 Evaluation Board.” [Online]. Available: http://www.vicorpower.com/documents/user_guides/vichip/ug_Analog_LV_HV_6123_BCM_EvalBoard.pdf. [Accessed: 09-Jul-2019].

[19] 4pcb.com, “PCB Trace Width Calculator.” [Online]. Available: https://www.4pcb.com/trace-width-calculator.html. [Accessed: 10-Jul-2019].

[20] IXYS, “DSSK 40-006B Schottky diode.” [Online]. Available: http://ixapps.ixys.com/DataSheet/L245.pdf. [Accessed: 12-Jul-2019].

[21] Vishay, “SUP90P06-09L pMOSFET.” [Online]. Available: http://www.vishay.com/docs/73010/73010.pdf. [Accessed: 11-Jul-2019].

[22] Infineon Technologies, “IRFSL7430PBF nMOSFET,” 2014. [Online]. Available: http://www.irf.com/technical-info/appnotes/an-994.pdf. [Accessed: 13-Jul-2019].

[23] Texas Instruments, “LM5050-1 OR-ing FET Controller,” 2011. [Online]. Available: http://www.ti.com/lit/ds/symlink/lm5050-1.pdf. [Accessed: 13-Jul-2019].

[24] Rak wireless, “Power Line Communication Module LX200V20.” [Online]. Available: https://www.rakwireless.com/en/module/plc/LX200V20. [Accessed: 13-Jul-2019].

[25] Wiskey, “WisPLC development board.” [Online]. Available: https://www.aliexpress.com/item/32791324046.html?storeId=2805180. [Accessed: 14-Jul-2019].

[26] Teledyne LeCroy, “WaveJet 324A Oscilloscope.” [Online]. Available: http://cdn.teledynelecroy.com/files/pdf/lecroy_wavejet-a_oscilloscope_datasheet.pdf. [Accessed: 13-Jun-2019].

[27] Mauch Electronics, “PL 2-6S Hall Sensor.” [Online]. Available: https://www.mauch-electronic.com/pl-2-6s-bec. [Accessed: 28-Feb-2019].

[28] Betaflight.com, “Flight controller software.” [Online]. Available: https://betaflight.com/. [Accessed: 18-Jun-2019].

[29] iperf.fr, “iPerf - The TCP, UDP and SCTP network bandwidth measurement tool.” [Online]. Available: https://iperf.fr/. [Accessed: 14-Jul-2019].

Appendix A

Extra measurements

A) ON 20 %

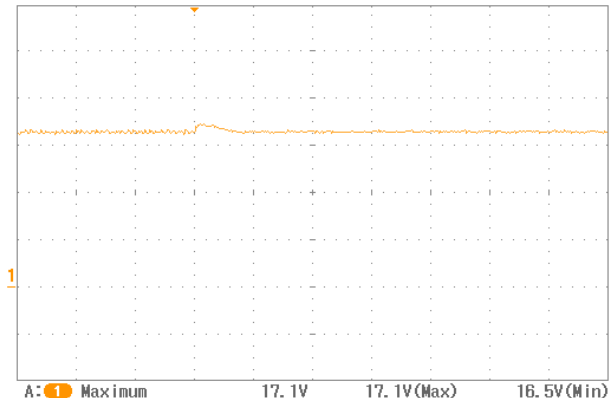

B) LF 20 %

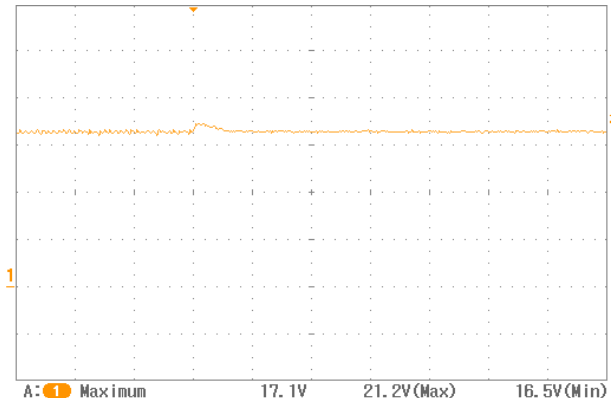

C) ON 40 %

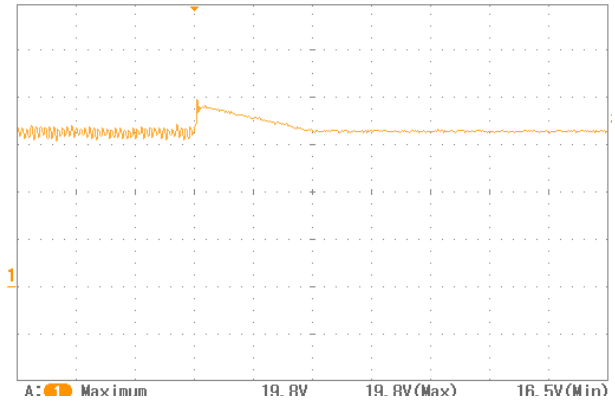

D) LF 40 %

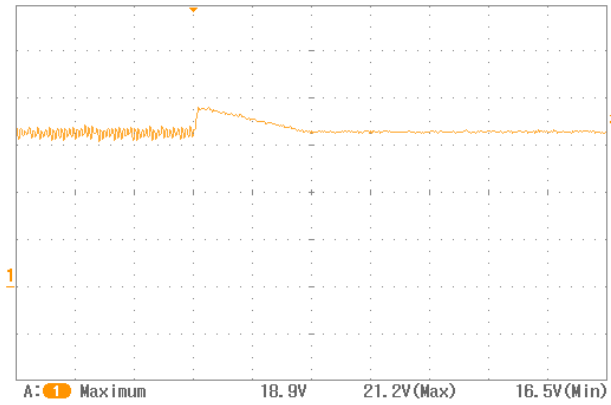

E) ON 80 %

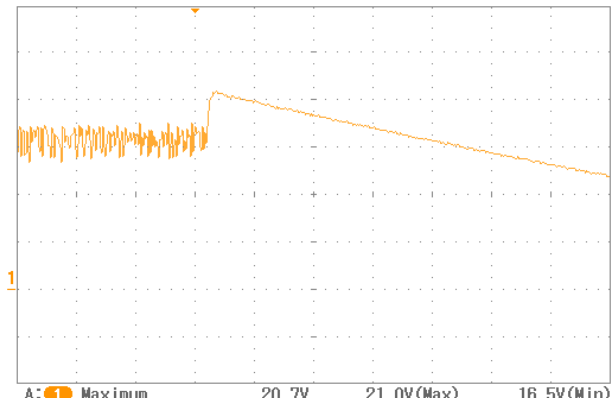

F) LF 80 %

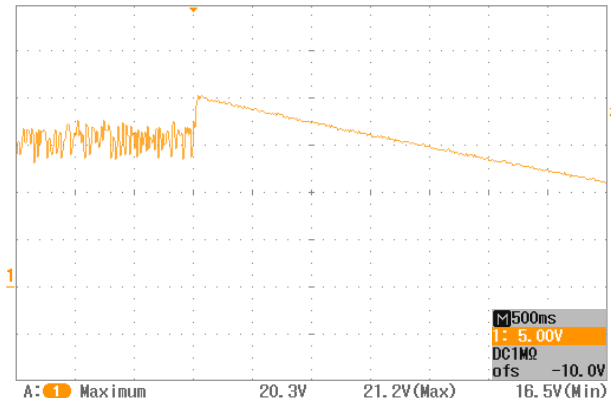

Figure A.1: Response from two different 20 V TVS diodes in parallel on 16.5 V / single 1700 Kv.

X-axis: Time [500 ms/div]. Y-axis: Voltage [5 V/div].

A) TVS + capacitor at 40 %

B) TVS + capacitor at 60 %

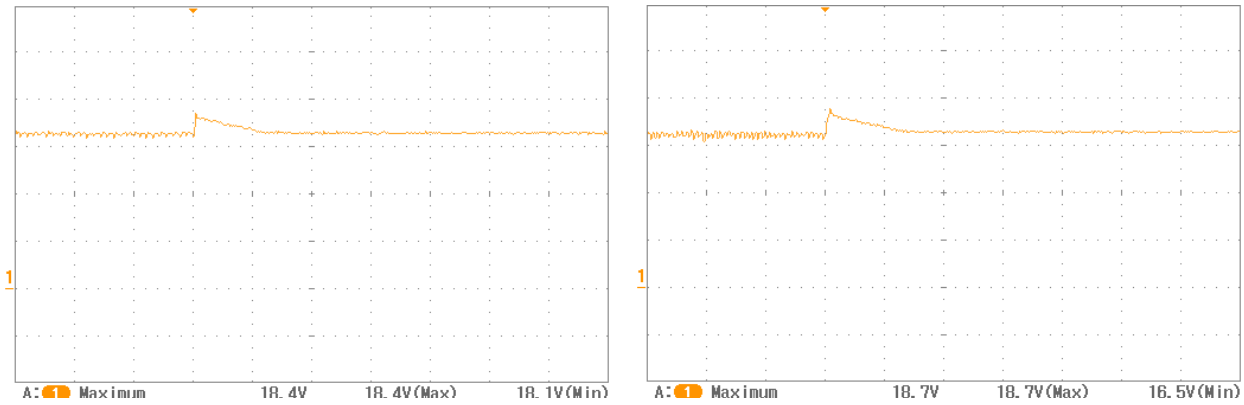

Figure A.2: 18 V TVS + 470 uF capacitor in parallel on 16.5 V / single 1700 Kv.

X-axis: Time [500 ms/div]. Y-axis: Voltage [5 V/div].

A) 1x TVS

B) 2x TVS

C) 3x TVS

D) 2x TVS + capacitor

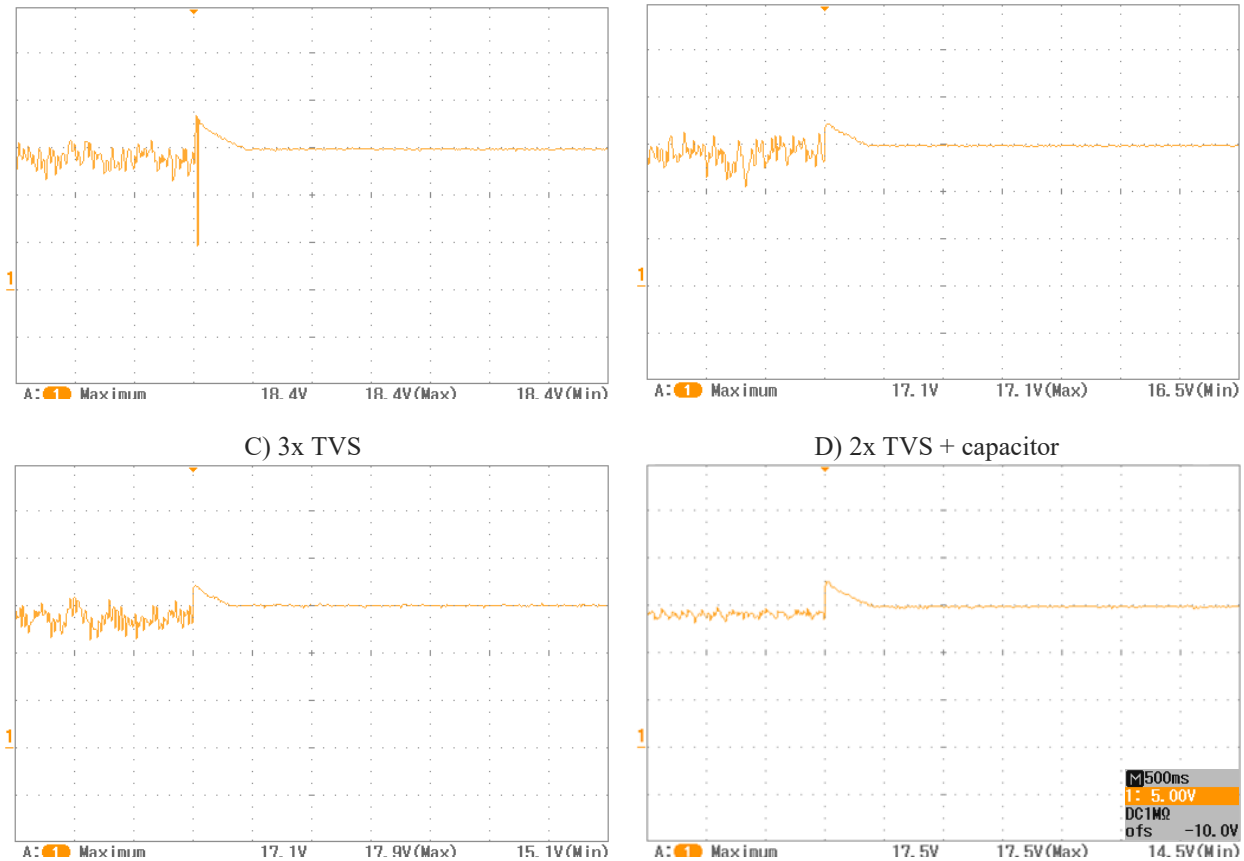

Figure A.3: Combinations of 16 V TVS diodes and 470 uF in parallel at 60 % on 15 V / Woody.

X-axis: Time [500 ms/div]. Y-axis: Voltage [5 V/div].

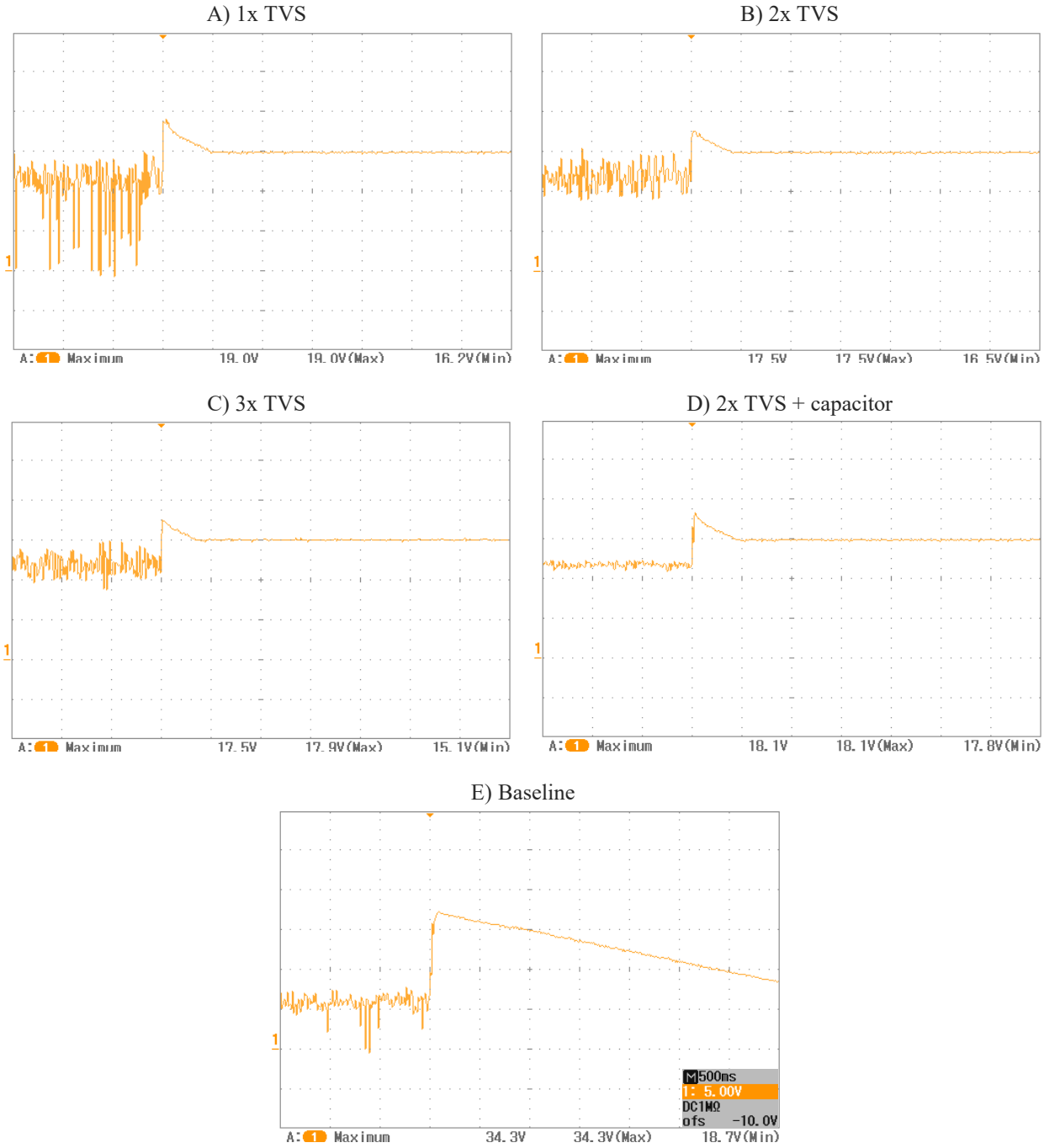

Figure A.4: Combinations of 16 V TVS diodes and 470 uF in parallel at 100 % on 15 V / Woody.

X-axis: Time [500 ms/div]. Y-axis: Voltage [5 V/div].

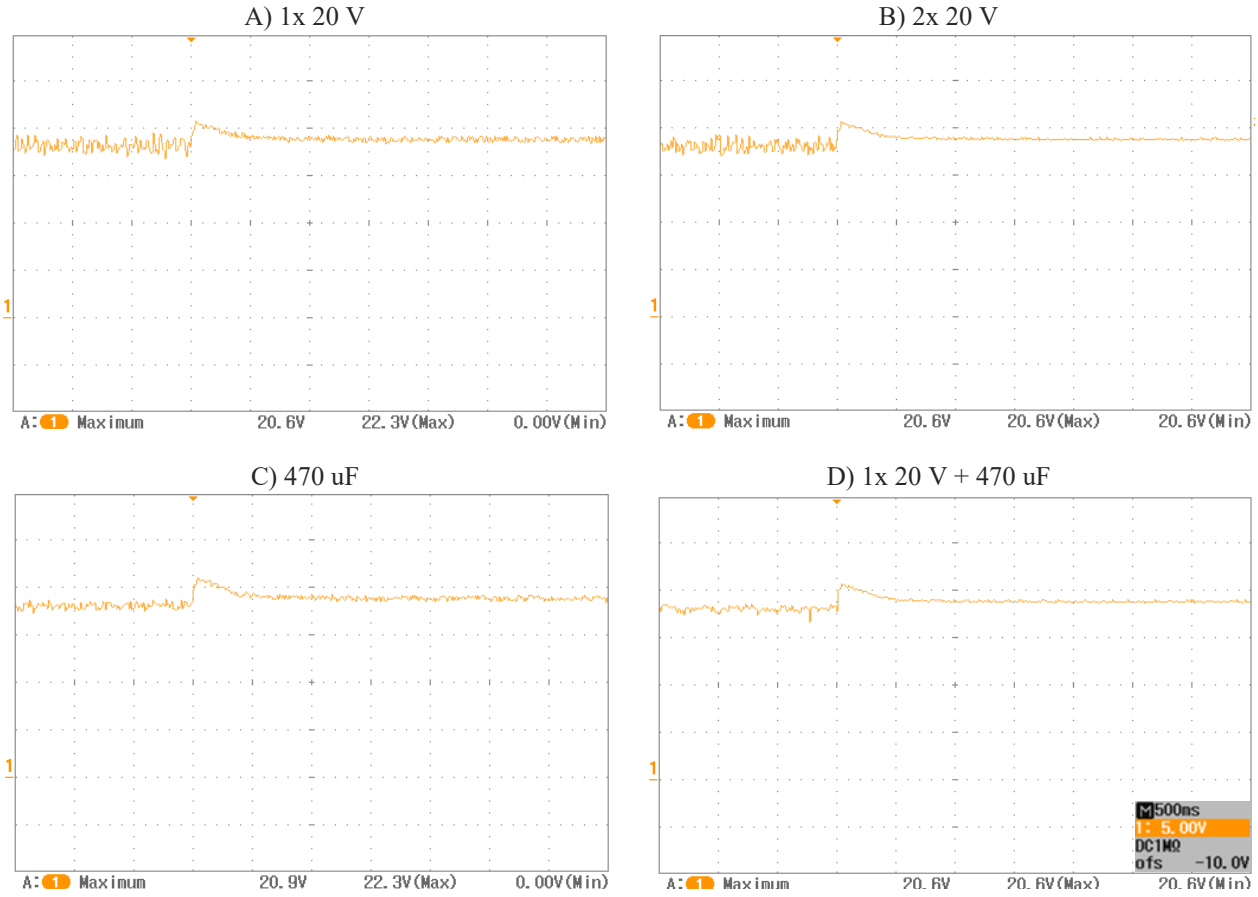

Figure A.5: Different configurations of TVS diodes and a capacitor on the ESC at 40 % thrust.

X-axis: Time [500 ms/div]. Y-axis: Voltage [5 V/div].

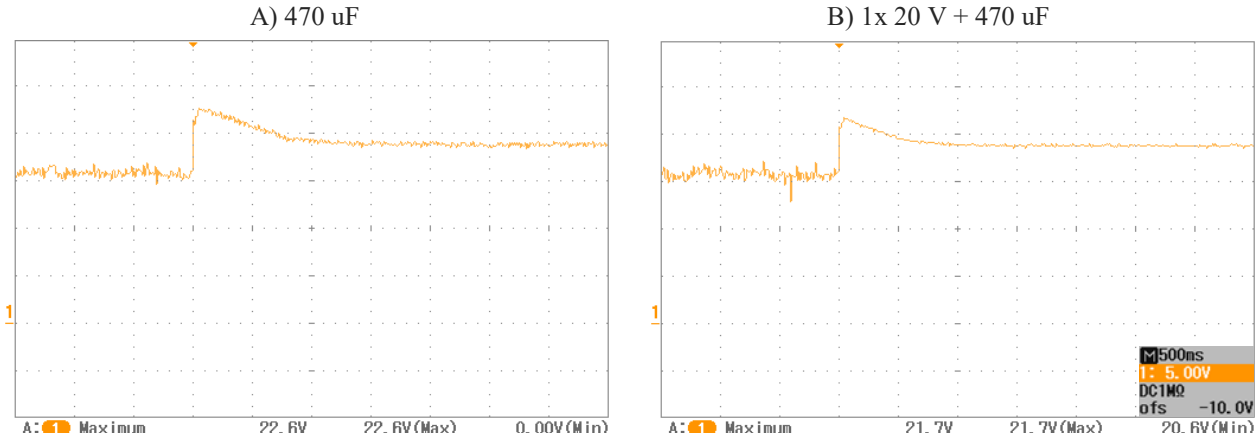

Figure A.6: Different configurations of TVS diodes and a capacitor on the ESC at 80 % thrust.

X-axis: Time [500 ms/div]. Y-axis: Voltage [5 V/div].

Table A.1: iPerf3 bandwidth results over 60 seconds on data link with PSU on (300 V, 0 A).

	Bandwidth [Mbit/s]	*Jitter [ms]*	*Lost/Total Datagrams*
No chokes	27.0	2.057	0/24718 (0 %)
PSU choke	63.7	0.965	0/58275 (0 %)
Two chokes	94.7	0.405	0/86683 (0 %)

Table A.2: iPerf3 bandwidth results over 60 seconds on data link with PSU off.

	Bandwidth [Mbit/s]	*Jitter [ms]*	*Lost/Total Datagrams*
No chokes	88.0	0.575	0/80559 (0 %)
PSU choke	92.9	0.582	0/85020 (0 %)
Two chokes	95.6	0.404	0/87526 (0 %)

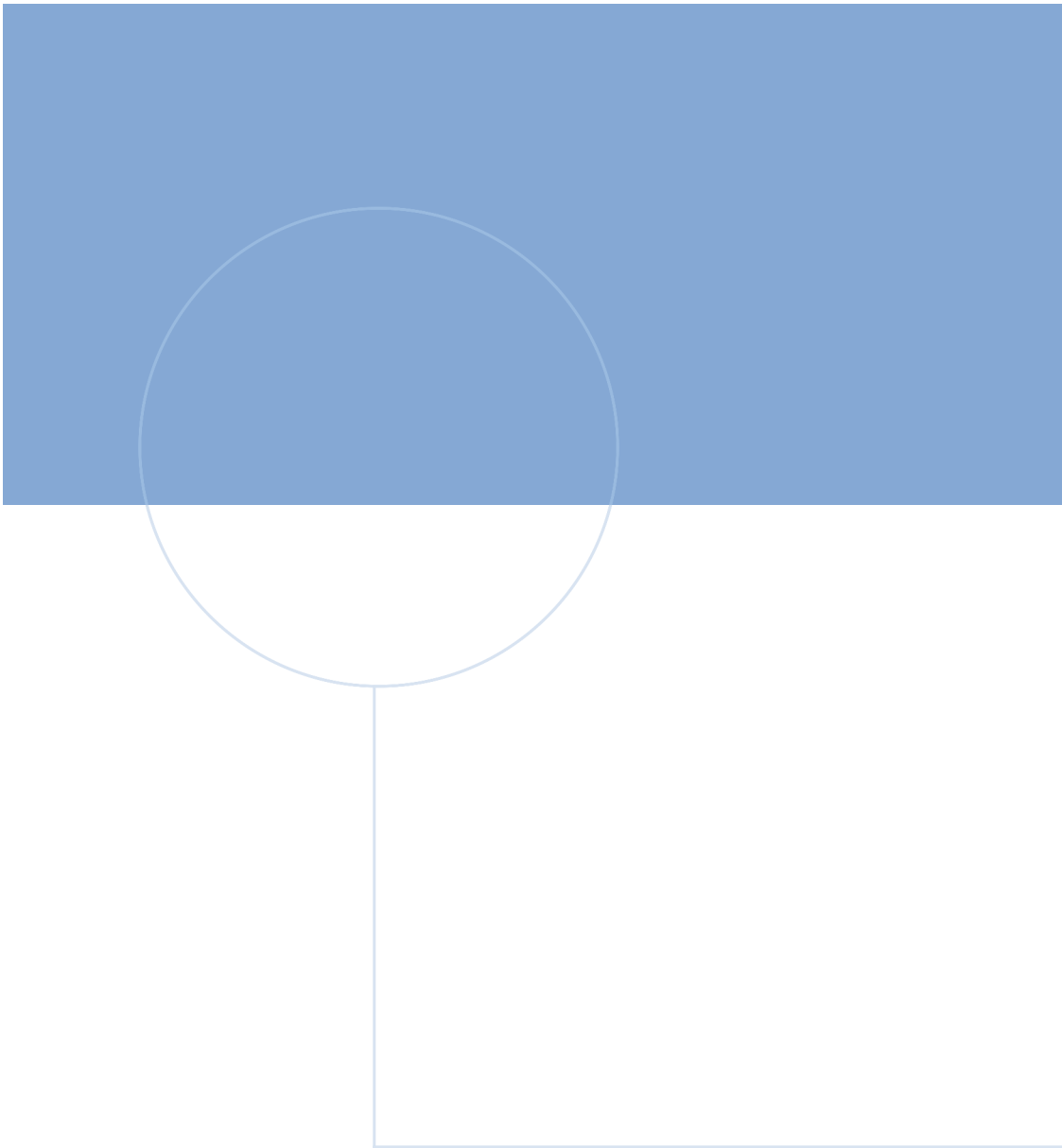

NTNU
Norwegian University of
Science and Technology